International Journal of Earth Sciences (2021) 110:809–832
https://doi.org/10.1007/s00531-021-01991-4

ORIGINAL PAPER

Ophicalcites from the Upper Tectonic Unit on Tinos, Cyclades, Greece: mineralogical, geochemical and isotope evidence for their origin and evolution

C. Mavrogonatos[1] · A. Magganas[1] · M. Kati[1] · M. Bröcker[2] · P. Voudouris[1]

Received: 5 October 2020 / Accepted: 11 January 2021 / Published online: 18 February 2021

Abstract
Ophicalcites exposed on the island of Tinos, Greece, occur as ellipsoidal bodies within greenschist-facies phyllites of the Upper Cycladic Unit. Close to their outcrops, blocks of serpentinites, metabasic rocks and metasediments were identified, implying a tectonically dismembered ophiolitic sequence in the study area. The ophicalcites comprise brecciated serpentinites cemented by calcite. Based on textural, mineralogical and deformation features, five ophicalcite varieties were discriminated, reflecting calcite precipitation, sedimentary features and increasing brecciation. Serpentinitic fragments comprise antigorite, while Cr-spinel, magnetite, talc and chlorite are accessory minerals. Carbonate veins consist of calcite and minor dolomite, talc, chlorite, and rarely epidote. Bulk rock chemical compositions and Cr-spinel mineral composition point towards a supra-subduction environment. Carbon and oxygen isotope ratios of calcite imply precipitation from mixed marine and hydrothermal fluids, followed by isotope exchange due to late, greenschist-facies overprint. The Tinos ophicalcites record intraoceanic exhumation of the ultramafics at the seafloor, where faulting and serpentinization caused an extensive network of fractures, healed by carbonates. Such intraoceanic deformation can be attributed either to obduction tectonics expressed by thrusting of oceanic piles, or to transpressional(?) transform faults, or more probably to slip along detachment fault of an oceanic core complex.

Keywords Ophicalcites · Tectonic mélange · Tinos Island · Attic-cycladic massif · Greece · Mantle exhumation · Intraoceanic deformation · Serpentinite

Introduction

Ophicarbonates are made of brecciated and serpentinized ultramafic fragments cemented by fracture-filling carbonates. Calcite is commonly the main carbonate mineral and thus, the term "ophicalcite" is often used to name these rocks (e.g., Spooner and Fyfe 1973; Cortesogno et al. 1981; Lagabrielle and Cannat 1990). Serpentinization of ultramafic rocks during exhumation and alteration of oceanic lithosphere causes volume expansion and extensive fracturing.

✉ C. Mavrogonatos
kmavrogon@geol.uoa.gr

1 Faculty of Geology and Geoenvironment, Section of Mineralogy and Petrology, National and Kapodistrian University of Athens, University Campus-Zografou, 15784 Athens, Greece

2 Institut für Mineralogie, Westfälische-Wilhelms Universität Münster, Corrensstr. 24, 48149 Münster, Germany

Serpentinization also releases hydrogen- and methane-rich fluids sometimes resulting in extensive precipitation of carbonates under moderate to low temperature conditions (e.g., Kelley et al. 2005; Allen and Seyfried 2003). The degree of fracturing, carbonation, reworking and subsequent redeposition of the carbonated ultramafic rocks is highly variable and leads to a variety of ophicalcite lithotypes. Based on their fabric, Tricart and Lemoine (1989) distinguished two main types of ophicalcites: the first variety (OC1) comprises serpentinitic breccias crosscut by carbonate and serpentine veins, that evolve downwards into massive serpentinite; the second type (OC2) is the product of submarine reworking, short-distance transport and subsequent redeposition of ultramafic 'conglomerates' and usually overlies the first type. In some cases, ophicalcites also include "exotic" clasts, like marbles, gneisses, and/or basaltic blocks (Bernoulli and Weissert 1985; Melfos et al. 2009; Clerc et al. 2014).

Ophicalcites were first described in the Ligurian and the Swiss Alps (Bonney 1879; Cornelius 1912), where they occur as constituents of Mesozoic ophiolitic sequences (e.g., Florineth and Froitzheim 1994; Bernoulli and Manatschal 2002; Bernoulli et al. 2003; Manatschal et al. 2003). Since then, they have been reported from many localities worldwide (cf. Artemyev and Zaykov 2010). The oldest known ophicalcites occur in a Precambrian ophiolitic sequences in Egypt (Surour and Arafa 1997) and the Ordovician of the Southern Quebec Appalachians (Lavoie and Cousineau 1995). They are also found in present-day settings, such as the Iberian margin, offshore Galicia (Whitmarsh et al. 1998; Boillot and Froitzheim 2001; Péron-Pinvidic and Manatschal 2009) and the Mid-Atlantic ridge (Kelley et al. 2005; Ludwig et al. 2006; Escartín et al. 2008; MacLeod et al. 2009).

Many theories have been proposed for the formation of ophicalcites, including the intrusion of ultrabasic magma into limestones (Cornelius 1912), contact or regional metamorphism of dolomites and limestones (Peters 1965; Trommsdorff et al. 1980), explosive (carbonatitic magma, Bailey and McCallien 1960) and pedogenic origins (Folk and McBride 1976), or disruption of serpentinitic rocks by methane seeps (Haggerty 1991). Recent studies, also based on drilling and observations at the modern ocean floor (e.g., IODP—International Ocean Discovery Project), related ophicalcite formation to a combination of fracturing, hydrothermal circulation and/or sedimentation, that take place in three major geotectonic settings (Fig. 1), namely the ocean to continent transition zones (OCT), oceanic core complexes (OCC) and along transform fault zones (e.g., Florineth and Froitzheim 1994; Lagabrielle and Lemoine 1997; Bernoulli and Manatschal 2002; Bernoulli et al. 2003; Péron-Pinvidic and Manatschal 2009; Picazo et al. 2012; Lafay et al. 2017).

During continental rifting, mantle lithologies can be exposed along large-scale faults with low magma input (Fryer 2012). Intense fracturing, hydrothermal alteration and reworking/redeposition of the exhumed ultramafics lead to the formation of ophicalcites at the so-called, OCT environment. Such examples include the western Alpine ophicalcites (e.g., Florineth and Froitzheim 1994; Manatschal and Müntener 2009) and the actualistic example of the Iberia-New Foundland rifted margins (e.g., Péron-Pinvidic and Manatschal 2009; Schwarzenbach et al. 2013; Klein et al. 2015). At (ultra-)slow-spreading oceanic ridges and usually close to transform fracture zones, ultramafic lithologies are exhumed along detachment faults in the amagmatic segments of the ridge, thus, forming corrugated megamullion structures, known as Oceanic Core Complexes (OCC, Cann et al. 1997; Ildefonse et al. 2007; Escartín et al. 2008; MacLeod et al. 2009). In such environments, the interaction of seawater with the exhumed ultramafic rocks enhances alteration and carbonate precipitation in the faulted peridotites (Cannat et al. 2006; Eickmann et al. 2009), as is the case for the Chenaillet ophicalcites in the Western Alps (e.g., Lagabrielle and Lemoine 1997; Lafay et al. 2017), or those dredged from the Lost City hydrothermal field in the Atlantis Massif of the Mid-Atlantic ridge (Kelley et al. 2005; Ludwig et al. 2006; Escartín et al. 2008; MacLeod et al. 2009). In such regime, ophicalcites may also form near the intersection of the ridge with large-scale transform faults (Lagabrielle and Cannat 1990; Picazo et al. 2012), as is the case for the Apennine ophicalcites (Lagabrielle and Cannat 1990).

In contrast to the previous impression that ophicalcites are absent from the eastern Mediterranean region (Bernoulli and Jenkyns 2009), Greece hosts at least five ophicalcite occurrences. All these occurrences are related to Mesozoic ophiolitic rocks and so far, remain poorly studied. One of the most important occurrences lies in the Chasanbali area on mainland Greece, from where the famous "Verde Antico" decorative stone was extracted during the antiquity (Paraskevopoulos and Kanaki 1973; Melfos et al. 2009; Kati et al. 2009). Other occurrences are located near Veria and Kozani,

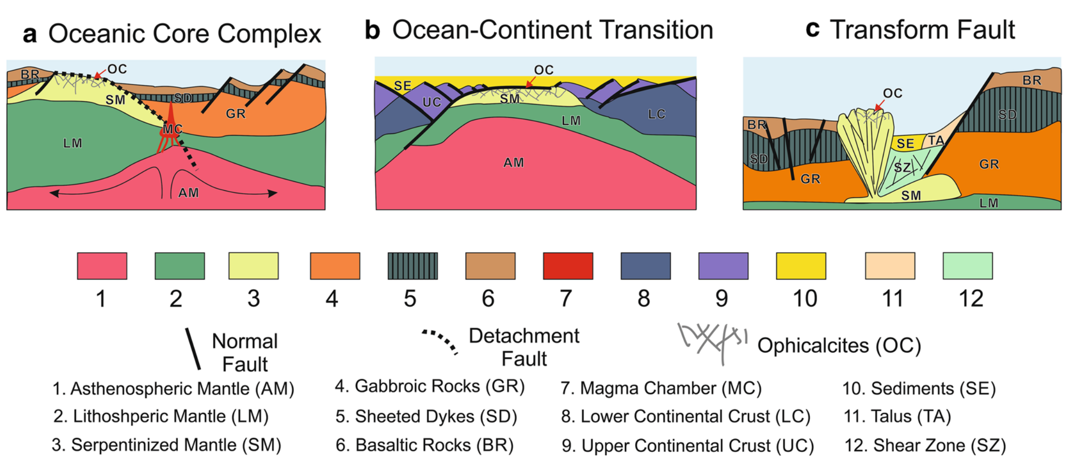

Fig. 1 Conceptual models of various geotectonic environments displaying the areas where ophicalcites form. Modified from Péron-Pinvidic and Manatschal (2009), Bach and Früh-Green (2010)

as well as on the islands of Evia, Tinos (Paraskevopoulos and Kanaki 1973), and Paros (Baltatzis 1984).

On Tinos, the ophicalcites occur within the Upper Cycladic Unit (UCU), closely associated with other mafic and ultramafic rocks, which together represent remnants of a dismembered ophiolitic complex (Katzir et al. 1996, 2007). Ophicalcites are exposed in the NW part of the island, where many outcrops and quarries are found ca. 3 km north of Marlas (Fig. 2c). Since ancient times, the famous “Verde di Tinos” stone is extracted from this area for building and decorative purposes, especially in monumental constructions, like St. Peter Basilica at the Vatican City. Despite their high commercial and historical value, the Tinos ophicalcites have not received much scientific attention and their field occurrence, mineralogy, geochemistry and their mode of formation are largely unknown. Previous studies on the Tinos ophicalcites only gave rather broad explanations for their formation including non-specified tectonic processes

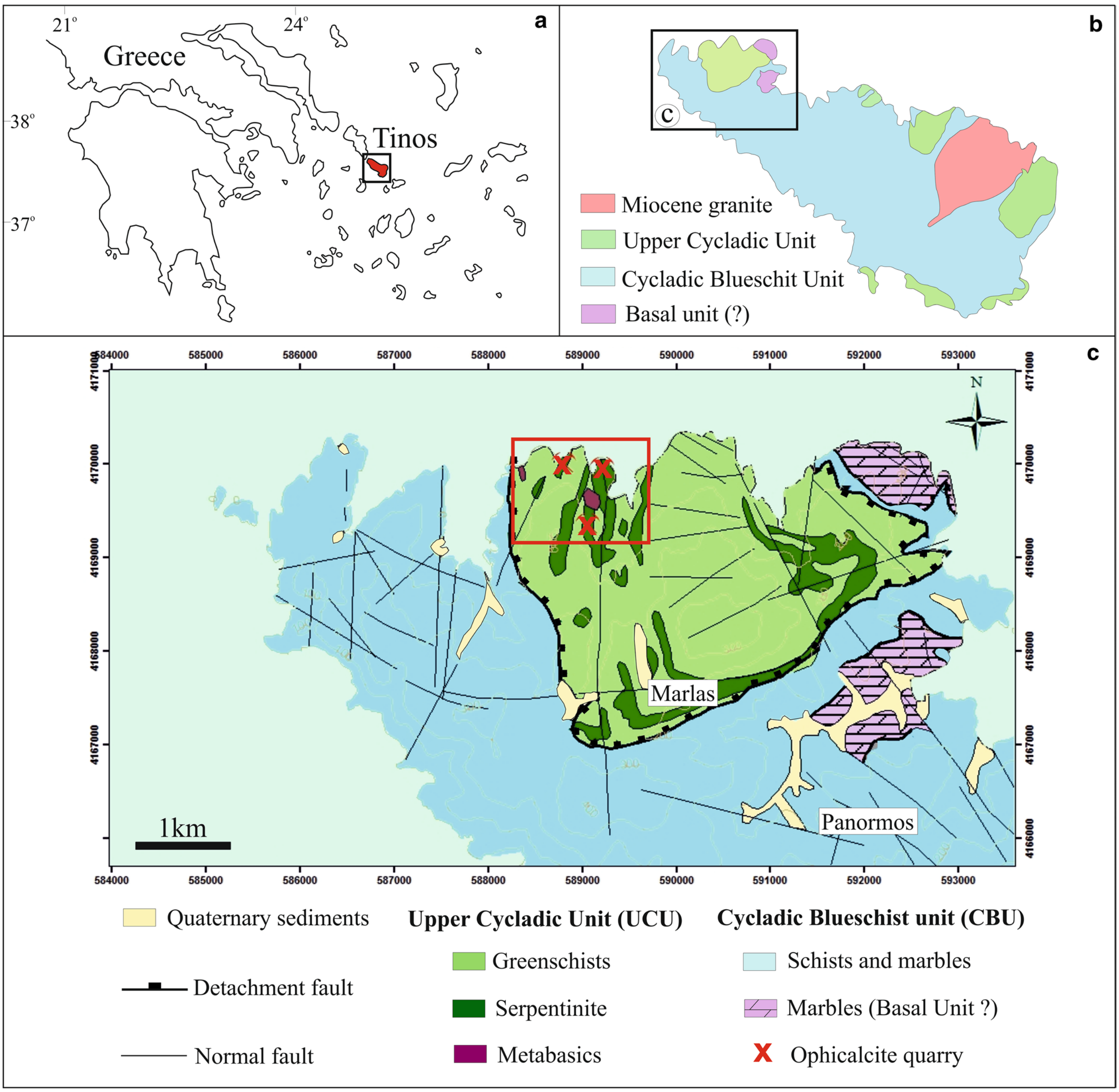

Fig. 2 **a** Geographic overview of the larger study area; **b** simplified geological map of Tinos island (modified after Melidonis 1980; Breeding et al. 2003); **c** detailed geological sketch map of the NW part of Tinos island, modified after the geological map of the Hellenic Survey of Geology and Mineral Exploration (Tinos-Yaros Sheet 2003). The red box marks the study area

(Papageorgakis, 1966), intrusion of ultramafic magma in carbonate rocks or reaction of $CaCO_3$-rich fluids with serpentinites (Paraskevopoulos and Kanaki 1973). The presence of fully carbonated ultramafic rocks (listvenites) in other parts of the Upper Cycladic Unit on Tinos (Hinsken et al. 2017) raises the question whether both rock types are genetically related, representing successive steps in the continuous carbonation of ultramafic rocks. We describe here in detail the geological, mineralogical and geochemical aspects of the ophicalcites and examine possible petrogenetic mechanisms and geodynamic settings for their formation.

Geological setting

Tinos island is part of the Cyclades archipelago (Fig. 2a, b), and geologically belongs to the Attic-Cycladic Massif (ACM). In the ACM, three major tectono-metamorphic units can be distinguished, separated by low-angle normal faults (e.g., Dürr et al. 1978). The presumed lowermost para-autochthonous unit is exposed in a few tectonic windows (e.g., Evia Island) and comprises Cenozoic metasedimentary rocks (Papanikolaou 1979; Katsikatsos et al. 1986; Avigad and Garfunkel 1989, 1991; Matthews et al. 1999). The Cycladic Blueschists Unit (CBU) tectonically overlies the lowermost unit and is a Mesozoic sequence consisting of marbles, calc schists, metaconglomerates, mica schists, quartzites and metavolcanic rocks (Melidonis 1980; Hinsken et al. 2017; Seman et al. 2017). In a few islands (e.g., Paros island), the CBU is locally underlain by Carboniferous granitic orthogneisses and granites, which constitute the Cycladic Basement (e.g., Engel and Reischmann 1998; Bargnesi et al. 2013). Metamorphic ages for the CBU mainly document an Eocene blueschist- to eclogite-facies episode, reaching P–T conditions of ca. 15 kbar and 450–500 °C (Matthews and Schliestedt 1984; Bröcker and Enders 2001; Okrusch and Bröcker 1990; Soukis and Stockli 2013). The importance of Cretaceous U–Pb zircon ages (ca. 80 Ma) that had been interpreted to indicate hydrothermal or metasomatic processes in a subduction zone environment, suggesting pre-Eocene HP/LT metamorphism (Bröcker and Enders 1999; Bröcker and Keasling 2006), was not confirmed by subsequent studies (Bulle et al. 2010; Fu et al. 2010). However, the existence of a NE-dipping subduction zone that operated already in Late Cretaceous time (74 ± 3.5 Ma) is indicated by formation of a metamorphic sole related to obduction of the Tinos ophiolite (Lamont et al. 2020). These authors also concluded that the Eocene HP/LT rocks are related to the same subduction zone.

Recent studies report higher metamorphic conditions for the blueschist–eclogite facies episode (ca. 20 kbar and 600 °C; Groppo et al. 2009; Dragovic et al. 2012, 2015; Ashley et al. 2014). A retrograde metamorphic event during Late Oligocene to Early Miocene accompanied the exhumation of the CBU, with estimated P–T conditions of ca. 4–7 kbar and 450–500 °C, causing extensive greenschist and locally amphibolite facies overprinting (e.g., Bröcker et al. 1993; Ring 2010; Philippon et al. 2011; Soukis and Stockli 2013).

The CBU is in turn tectonically overlain by the Upper Cycladic Unit (UCU), which actually comprises the hanging wall of a detachment faults system (Jolivet and Patriat 1999; Sánchez-Gómez et al. 2002), known as North Cycladic Detachment System (NCDS) (Gautier and Brun 1994a, b; Jolivet and Patriat 1999; Sánchez-Gómez et al. 2002; Brichau et al. 2007; Jolivet et al. 2010, 2013; Soukis and Stockli 2013). All rock types of the UCU have escaped the HP/LT event that affected the CBU and experienced greenschist (rarely up to medium amphibolite) facies metamorphism (Maluski et al. 1987; Patzak et al. 1994; Katzir et al. 1996; Sánchez-Gómez et al. 2002; Soukis and Papanikolaou 2004).

Tinos island is mostly built up by lithologies of the CBU (Fig. 2b, c): various types of metasedimentary and metabasic schists and marbles predominate; metabasic blocks that are scarcely embedded in this succession imply an olistostromatic character for large parts of this unit (Bulle et al. 2010). Despite the pervasive greenschist-facies overprint, relict blueschist assemblages are often preserved (Melidonis 1980; Bröcker et al. 1993; Breeding et al. 2003). At its lower part, the CBU on Tinos comprises dolomitic marbles and minor phyllites. This sequence has been interpreted either as an integral part of the CBU (e.g., Melidonis 1980; Bröcker and Franz 2005), or as a para-autochthonous sequence known as the Basal Unit (Avigad and Garfunkel 1989), which is tectonically overlain by the CBU in the area of Panormos (Fig. 2c). The UCU on Tinos Island has restricted surface outcrops (Fig. 2b, c) and reaches a maximum thickness of about 500 m. It comprises mafic and ultramafic lithologies including serpentinites, metagabbros, ophicalcites, listvenites, talc schists, and phyllitic rocks with greenschist-facies mineral assemblages (Melidonis 1980; Katzir et al. 1996; Bröcker and Franz 1998; Zeffren et al. 2005; Mavrogonatos et al. 2014, 2015; Hinsken et al. 2017). Occasionally, metasedimentary rocks (meta-cherts and meta-clastic rocks) also occur as blocks. In contrast to the meta-ophiolitic rocks occurring in the upper levels of the CBU (e.g., northern Syros), which are interpreted to be parts of the Mesozoic Pindos sub-oceanic lithosphere, the ophiolitic material of the UCU is believed to originate from the Vardar oceanic strand (Jolivet et al. 2010).

Previous studies suggested an Upper Cretaceous metamorphic age for the UCU ophiolitic rocks on Tinos (Zeffren et al. 2005; Katzir et al. 2007). Katzir et al. (2007) argued for a Upper Cretaceous age, based on hornblende K–Ar data for an amphibolite–gneiss block, from the topmost part of the Tinos tectono-metamorphic sequence (Patzak et al. 1994).

However, it remains speculative whether this age represents the metamorphic sole of the obducted meta-ophiolite or is just the age of a distinct tectonic unit (Akrotiri Unit) on top of the UCU (e.g., Patzak et al. 1994). Similar metamorphic and/or magmatic ages were reported from the UCU exposed on other Cycladic islands (e.g., Patzak et al. 1994; Be'eri-Shlevin et al. 2009; Martha et al. 2016 and references therein).

The protolith age of the ultramafic–gabbroic rock suite has recently been constrained by U–Pb zircon geochronology of samples from the Tsiknias area, East Tinos. A plagiogranite yielded an age of 161.9 ± 2.8 Ma; a gabbro intruding this rock was dated at 144.4 ± 5.6 Ma (Lamont et al. 2020).

The Tsiknias occurrence is underlain by a metamorphic sole which contains anatectic amphibolites, pelagic metasediments and mafic phyllites that record an inverted metamorphic gradient (Lamont et al. 2020). Leucosomes from the uppermost sole amphibolite provided a U–Pb zircon igneous crystallization age of ~ 190 Ma and a high-grade metamorphic age of 74.0 ± 3.5 Ma, indicating a ca. 90 Ma age discrepancy between the ophiolite and the metamorphic sole (Lamont et al. 2020). Limited and not well-constrained metamorphic ages (Rb–Sr on phengite–whole rock and K–Ar on white micas) reported for phyllites/phyllonites range from ca. 92 to 21 Ma with a younging trend towards the tectonic contact between UCU and CBU (Bröcker and Franz 1998; Zeffren et al. 2005).

Tectonic juxtaposition of the UCU onto the CBU on Tinos has been dated at ca. 23–21 Ma (Rb–Sr phengite–whole rock, Bröcker and Franz 1998), being roughly contemporaneous with the greenschist-facies overprint of the underlying CBU. P–T conditions of ca. 450 °C and 4–7 kbar have been reported for both the UCU and the CBU during this Miocene event (e.g., Katzir et al. 1996; Bröcker and Franz 1998).

In the eastern part of the island, a granodiorite and associate leucogranitic bodies intrude both the CBU and the UCU (Avigad and Garfunkel 1989; Jolivet et al. 2010). K–Ar, Ar–Ar, Rb–Sr and U–Pb geochronology indicate middle Miocene crystallization ages (~ 14.5 Ma) for the magmatic rocks (Altherr et al. 1982; Bröcker and Franz 1998; Brichau et al. 2007).

Analytical methods

A total of 80 rock samples collected from the ophicalcites and the surrounding rocks of the UCU were used for petrographic, mineralogical and geochemical studies. From these samples, 60 thin sections underwent detailed petrographic investigation using optical microscopy. Quantitative analyses of mineral phases were conducted at the University of Athens, Department of Geology, using a JEOL JSM 5600 scanning electron microscope, equipped with automated OXFORD ISIS 300 energy dispersive analysis system. Analytical conditions were 20 kV accelerating voltage, 0.5 nA beam current, < 2 μm beam diameter and counting time of 10 s for peaks and 5 s for the background signal. The following X-ray lines were used: AsLα, FeKα, NiKα, CoKα, CuKα, CrKα, AlKα, TiKα, CaKα, SiKα, MnKα, MgKα. Standards used were pure metals for the elements Cu, Ni, Co and Cr, indium arsenide for As, pyrite for S and Fe, albite for Si, CaF_2 for Ca, MgO for Mg, Al_2O_3 for Al. Bulk rock powders of 27 samples were processed by X-ray diffraction, using a Bruker (Siemens) 5005 X-ray diffractometer, in conjunction with the DIFFRACplus software. Results were evaluated using the EVA 10.0 software. Serpentine polymorphs were discriminated using the criteria suggested by Whittaker and Zussman (1956). Chemical analyses of 11 rock samples were conducted by ICP-MS at ACME laboratories in Canada. For 8 calcite samples, stable isotope (C, O) analyses were performed at the laboratories of the Friedrich-Alexander Universität in Erlangen-Nürnberg, Germany. Carbonate (calcite) powders were reacted with 100% phosphoric acid at 70 °C using a Gasbench II machine connected to a ThermoFinnigan Five Plus mass spectrometer. All values are reported in per mil relative to VPDB by assigning $\delta^{13}C$ and $\delta^{18}O$ values + 1.95‰ and -2.20‰ to NBS19 and − 46.6‰ and − 26.7‰ to LSVEC, respectively. Reproducibility and accuracy were monitored by replicate analyses of laboratory standards calibrated to NBS19 and LSVEC and is better than ± 0.05 for $\delta^{13}C$ and ± 0.07 for $\delta^{18}O$.

Results

Field and structural observations

The Upper Cycladic Unit

One of the most important outcrops of the UCU on Tinos island occurs near Marlas, in the NW part of the island. This is the area where ophicalcites had been mined in large quarries (Figs. 2c, 3). The contact between the UCU and the underlying CBU is marked by intense shearing along the Tinos detachment fault. The meta-ophiolitic rock suite of the UCU is structurally built up by a succession of ultramafic and mafic slices that are separated by low-angle shear zones, subparallel to the main Tinos detachment, and more rarely by steep normal faults. Around Marlas, variably carbonated serpentinites and epidote–albite–chlorite-rich phyllites predominate (in the following referred to as "greenschists"), while metagabbros, metapyroxenites, talc schists, chromitites and metasedimentary rocks are only of subordinate importance. Field observations and cross-cutting relations

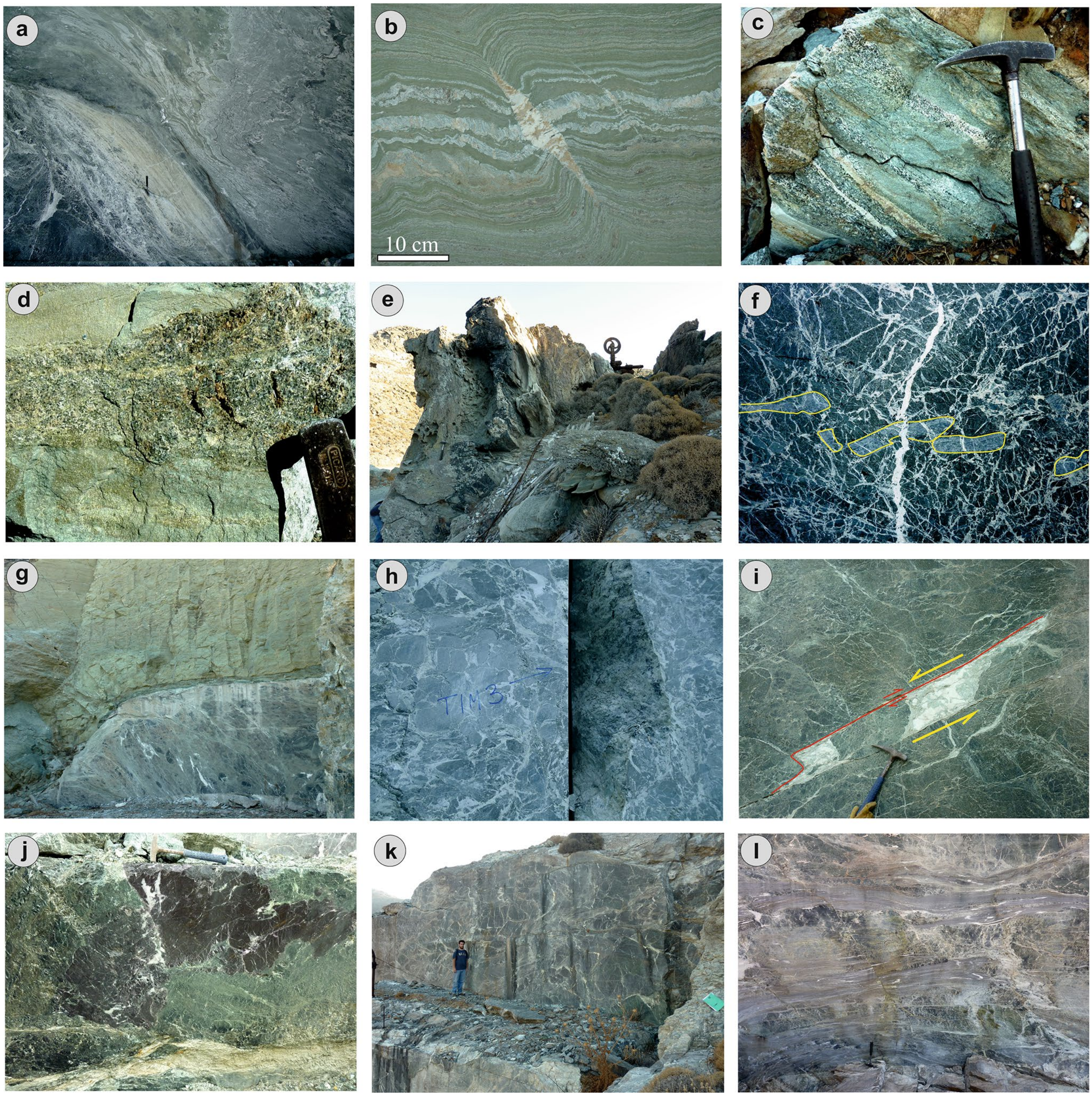

Fig. 3 Field photographs from the Tinos ophicalcites and related rocks. **a** Highly sheared contact between the ophicalcite (left side of the picture) and the greenschists; **b** double-sided mullions in greenschists; **c** banded, coarse-grained metagabbroic rocks; **d** layered metapyroxenite; **e** silicified Mn-rich metasediments enclosed in the greenschists; **f** Disrupted and subsequently imbricated serpentinized ultramafic dyke (former pyroxenite?, marked with yellow line) set in the cataclastic ophicalcite; **g** Matrix-supported serpentinitic breccia (serpentinitic mélange, lower part of the picture) enclosed in the greenschists (upper part of the picture); **h** Cataclastic ophicalcite with numerous, randomly oriented calcite veins; **i** Dilational jog in the cataclastic ophicalcite (the arrows indicate the sense of shear); **j** Chromitites affected by carbonation, enclosed in the cataclastic ophicalcite; **k** Mega-clastic ophicalcite; **l** Mylonitic ophicalcite: at places, m-scaled normal faults disrupt the shear zones

indicate that brittle deformation prevails in the structurally lower part of the succession, which is dominated by ultrabasic rocks; whereas, the overlying metabasic and metasedimentary lithologies exhibit a ductile to brittle–ductile fabric: two successive penetrative foliations and a prominent NE-trending stretching lineation, the latter being attributed to the North Cycladic Detachment System (NCDS) and the Oligo-Miocene exhumation, overprint an older coarse-grained foliation related to regional greenschist-facies metamorphism (Avigad and Garfunkel 1991; Patriat and Jolivet 1998; Zeffren et al. 2005; Brichau et al. 2007; Jolivet et al. 2010). It is noteworthy that the brittle deformation is restricted to the ultrabasic lithologies and does not affect or overprint the ductile fabric. A late-stage NE-trending, extension-parallel folding has created large-scale synforms and antiforms (Avigad et al. 2001). In addition to the km- or less-scaled folds, the existence of high- and low-angle extensional faults is responsible for a great variance (from 0° to ~ 90°) in the dip of the foliation planes of the greenschists.

The greenschists are mostly laminated and their total thickness is estimated to be more than 300 m. At places, increase of their chlorite content results in a glossy appearance. Close to the contact with the ultramafic rocks, the greenschists sometimes display a highly deformed texture (Fig. 3a). Locally up to 50 cm thick, non-coaxial boudins or double-sided mullions were observed, filled with calcite, albite, quartz, hematite ± chlorite (Fig. 3b). At some places, albite–hematite–chlorite–calcite–quartz segregations occur in domino-like shearing structures, oblique to the foliation of the epidote-rich greenschists.

Irregular-shaped blocks of massive metabasic rocks are found as large, elongated slices (up to 30 m thick) in the greenschists, mainly in the NW part of the Marlas area. Two major, strongly overprinted lithologies can be distinguished, cumulate metagabbroic rocks and metapyroxenites, now mostly consisting of amphiboles set in a matrix of albite, epidote, chlorite and quartz (Mavrogonatos et al. 2015). Metagabbroic rocks (Fig. 3c) are compositionally banded, and consist of leucocratic and melanocratic stripes; whereas, metapyroxenites either form layers enclosed in other mafic lithologies or appear as massive blocks with a maximum diameter of about 4 m (Fig. 3d). Occasionally, layers of Mn-rich metasediments (meta-clastic rocks and meta-cherts) occur as blocks in the greenschists (Fig. 3e) and form elongated bodies (up to 3 m in size).

Serpentinite is one of the main lithologies in the Marlas area occurring as large bodies (size up to 1 km) randomly distributed in a schistose matrix. Variably fractured and carbonated occurrences of such rocks constitute the ophicalcite deposits, which show an irregularly dense and varied network of calcite veins and veinlets in an ultramafic matrix. Sheared and non-carbonated serpentinitic bodies (up to a few meters thick) were recognized close to the contact with the CBU. Talc-rich zones (up to a few meters thick) often are developed at the contacts between serpentinites and greenschists. Formation of these zones most likely is related to deformation and metasomatic alteration during the greenschist-facies metamorphic episode. However, the talc-rich shear zones inside the ophicalcites, which do not extend beyond the borders of individual ophicalcite lenses may record evidence of early deformation, which is unrelated to the metamorphic fabric of the hosting greenschists. Rarely, disrupted veins of fine-grained serpentine (up to ca. 10 cm thick) crosscut the ultramafic rocks (Fig. 3f).

The ophicalcite occurrences

The ophicalcites consist of large masses of tectonized serpentinite with carbonate veins that occur as elongated caprocks or pod-shaped lenses (approximately 0.5 km across their long axis), or they constitute the deeper part of the succession. The ophicalcite bodies generally follow the NE-trending folding direction of the surrounding phyllitic greenschists and are usually located at the hinges of km- to dm-scaled anticlines. In cases where vertical faults are developed along the axial plane of the folds, the dip of the rock layers surrounding the faults increases accordingly. The transitional zone from the greenschists to the ophicalcites is usually marked by intense shearing and the presence of talc schists of varying thickness and chlorite-rich blackwall zones. The rarely exposed black-wall zones are highly sheared, and mainly consist of chlorite, actinolite, quartz, calcite, garnet and pyrite. Detailed field work led to the discrimination of five ophicalcite varieties (Fig. 3f–l) based on:

(a) the mechanism of formation (tectonic or tectonic ± sedimentary),
(b) the intensity of deformation, and
(c) the size and ratio between carbonate veins, serpentinite fragments and matrix.

Field relationships of these different types are presented in five schematic lithostratigraphic columns that are based on field observations (Fig. 4).

Carbonate-poor ophicalcite This type represents the least fractured type of the Tinos ophicalcites and is rarely exposed. It comprises massive serpentinites with minor calcite-filled veinlets or vugs. Towards the upper parts of these bodies, shear zones (up to a few cm thick) with a top-to-the-N or -NE sense of shear are relatively common.

Mylonitic ophicalcite This type has restricted outcrops and is represented by porphyroclastic, mylonitic and rarely ultramylonitic shear zones (ranging in thickness from a few centimeters up to 1 m), which commonly have a reddish to brown color, due to staining by Fe-oxides. Locally, the shear zones include lenses of less and/or almost undeformed serpentinite. Kinematic indicators such as S/C clasts and asymmetric boudin structures, mantled σ or δ calcite and serpentine porphyroclasts, show a top-to-N or -NE sense of shear. Extensional micro-faults (Fig. 3l) were also recognized at places.

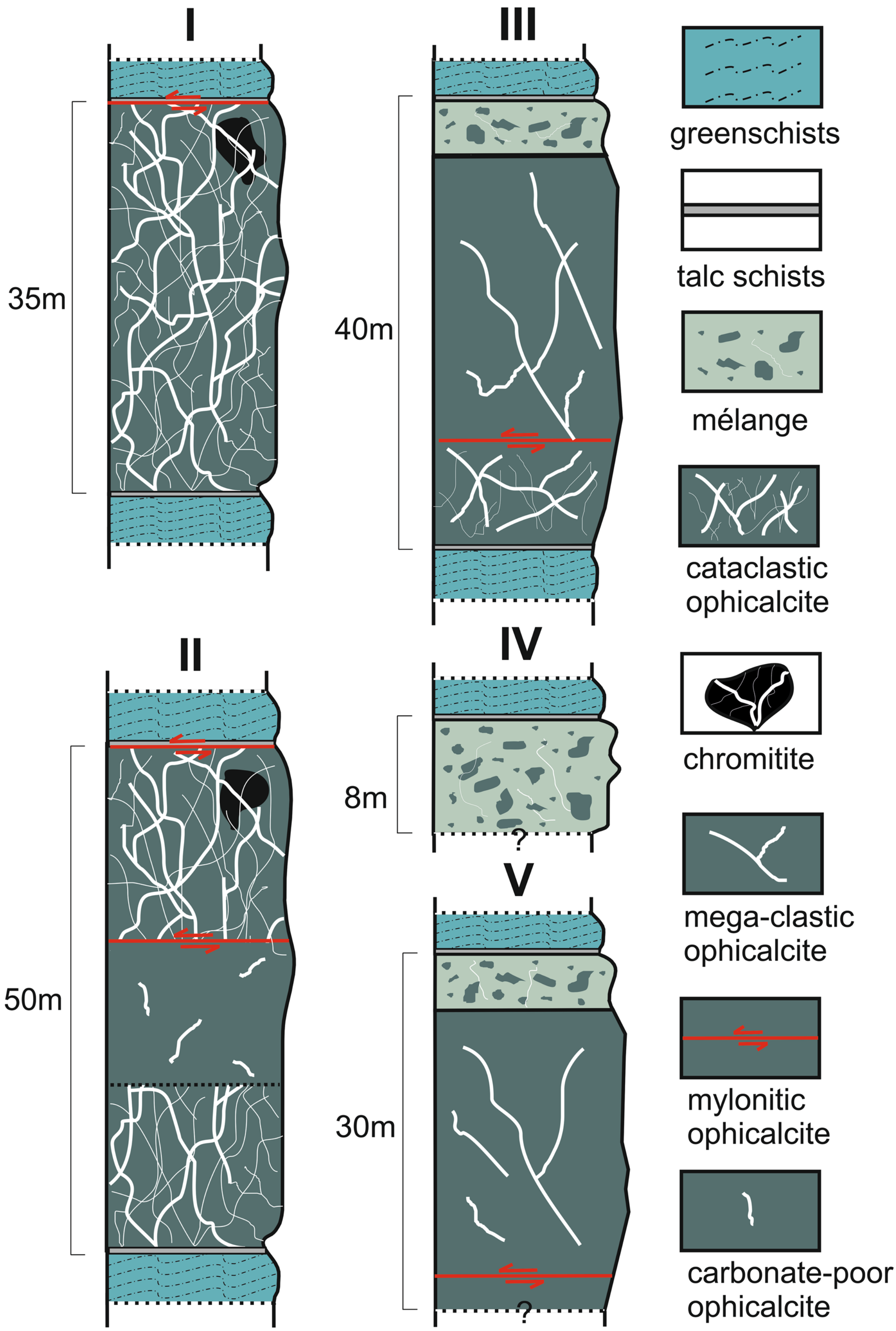

Fig. 4 Schematic tectonostratigraphic columns of the NW Tinos ophicalcites. Latin numbers refer to different ophicalcites occurrences

Mega-clastic ophicalcite This variety represents a type of tectonically fractured serpentinite, with ultramafic fragments significantly larger in dimensions compared to those of other cataclastic types (up to a few meters). Carbonate fracture fillings are randomly oriented in almost planar surfaces and are volumetrically much less than in other cataclastic types. They separate the main serpentinitic body into large angular to sub-angular, m-sized blocks, with no, or minor internal carbonate component (Fig. 3k). The angular blocks tend to become smaller in size and more round-shaped towards the marginal parts of such occurrences. Similarly, the proportion of fine-grained serpentinitic matrix increases, whereas the carbonate material decreases.

Cataclastic ophicalcite This textural variety represents the most widespread ophicalcite type and comprises a cohesive and cataclastic serpentinite breccia, with homogeneously sized clasts and numerous polygenetic carbonate and rarely serpentine, veins (Fig. 3h). The serpentinitic clasts are commonly angular, and have a mean size between 3 and 6 cm. Most of the carbonate veins show random orientations. Cross-cutting relations indicate at least three major generations of veins. The most distinct one consists of coarse-grained calcite and shows a quite systematic orientation, in some cases roughly parallel to the foliation of the greenschists. Reworked veins with angular carbonate clasts and/or small (< 1 cm) fragments of serpentinite are observed and can be attributed to pre-existing carbonate veins that were fractured during subsequent deformation. Calcite occurring along with fine-grained serpentinitic debris within rare dilational jogs (Fig. 3i) is probably related to a late event as well. Within the cataclastic ophicalcite, large pod-like or irregular shaped chromitites (Fig. 3j) occur (up to 5 m in length and 1 m in thickness). They are crosscut by numerous calcite veins with random orientation, similarly to the host serpentinites and, to our knowledge, such rock type has never been reported in the literature. They are commonly rimmed by a narrow zone (less than 0.5 m) consisting of fine-grained serpentinite, implying the existence of a dunitic envelop prior to serpentinization. Top-to-NE shear zones locally developed within the cataclastic ophicalcite type, leading to a highly sheared, mylonitic fabric in such domains.

Serpentinitic mélange This rock type can be found next to the highly sheared contact with the greenschists, but is rarely exposed (Figs. 3g, 4). It consists of a matrix-supported serpentinitic breccia crosscut by a few calcite veins. Unsorted, well-rounded clasts of serpentinite, ophicalcite and more rarely carbonates are enclosed in a fine-grained white to greenish matrix of serpentine, talc and carbonate minerals (Fig. 3i). The cross-cutting carbonate veins show no specific orientation. Sporadically, the matrix is red-colored, due to the presence of Fe-oxides (hematite staining).

Petrography

Greenschists/Phyllites

This rock type mainly consists of epidote, albite, actinolite, titanite and chlorite, with minor opaque minerals (magnetite, hematite, and pyrite), white mica and quartz. Greenschists are characterized by a lepidoblastic texture and the abundance of epidote (Fig. 5a, b), usually present as small anhedral grains, spheroidal aggregates or replacing feldspars. Albite forms small (up to 0.5 mm) anhedral grains that carry inclusions of other minerals, mainly actinolite and epidote, while quartz is rare. Actinolite forms mainly fibrous or acicular crystals with no systematic orientation, whereas titanite is present as idiomorphic grains with sizes smaller than 0.1 mm that in some cases grow around rutile cores. White mica (< 0.2 mm) is mostly found in association with actinolite and epidote.

Metagabbros and metapyroxenites

Both lithologies are characterized by intense porphyroblastic texture. Porphyroblasts (crystal sizes up to 30 mm) are mainly amphiboles, replacing primary magmatic pyroxene crystals (Fig. 5c, d). Replacement takes place along cleavage planes and/or at the periphery of the crystals and displays two stages, where pyroxene (augite) is first replaced by hornblende and later by actinolite. The matrix mainly consists of albite and quartz grown in a dense granoblastic texture. Accessory phases include epidote, clinozoisite, titanite, pumpellyite and opaques.

Talc schists

They consist of fine-grained aggregates of talc (up to 90%); whereas magnetite, tremolite, chlorite and opaque minerals (mostly magnetite and hematite) are the main accessory phases.

Chloritite

The chloritite (black-wall zone) sample is mainly composed of chlorite, actinolite, plagioclase and minor quartz, garnet and white mica. Commonly, it contains large (up to a few cm) euhedral crystals of pyrite.

Metasediments (meta-clastic rocks and Mn-rich meta-cherts)

Metaclastic rocks are composed of alternations of quartz-rich (± plagioclase) layers with zones dominated by white micas, which define the foliation. Minor calcite is also present as interstitial phase between quartz grains. The

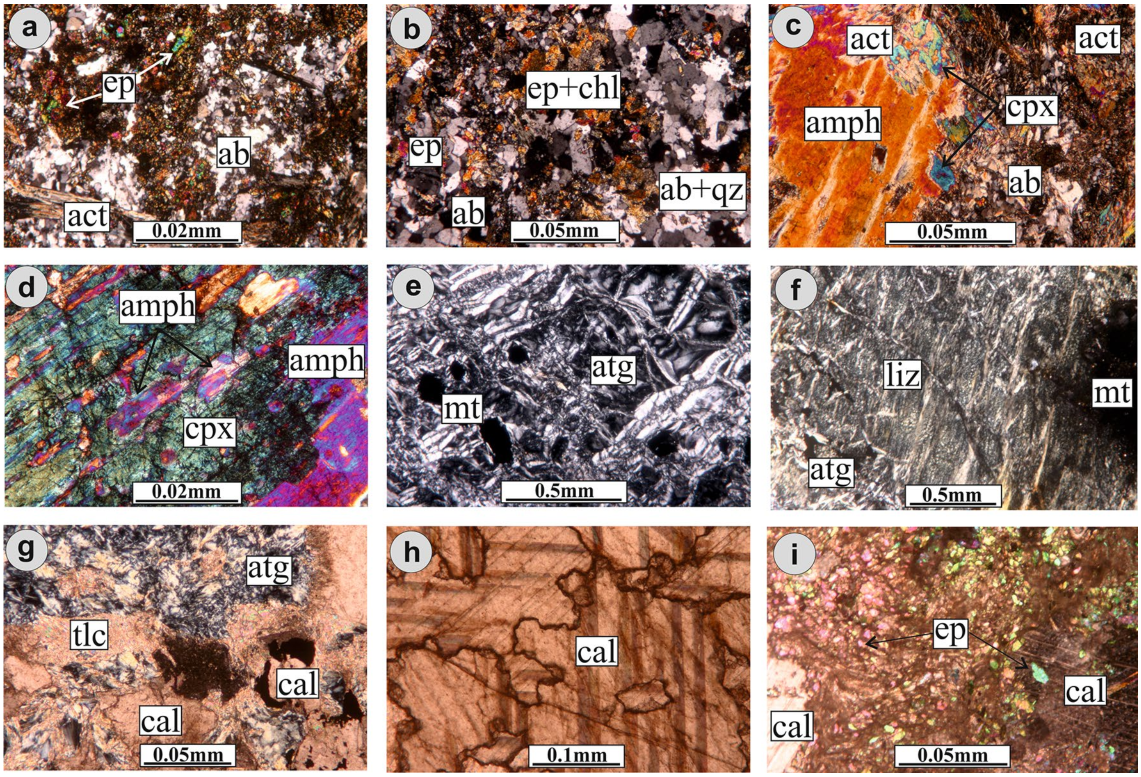

Fig. 5 Optical microscope (transmitted, crossed-polarized light) photographs from mineral associations of the ophicalcites and associated rocks from Tinos island: **a**, **b** Typical texture of greenschists with epidote (ep), albite (ab), chlorite (chl), actinolite (act) and quartz (qz); **c** Metagabbro showing a hornblende (amph) pseudomorph crystal (after pyroxene) being replaced by actinolite (act); **d** Metapyroxenite with characteristic amphibole (amph) replacement after clinopyroxene (cpx) along cleavage plains; **e** Hourglass texture formed by needle-shaped antigorite (atg) crystals in serpentinite; **f** Bastite formed by lizardite surrounded by antigorite (atg); **g** Calcite (cal) and talc (tlc) replacing antigorite (atg); **h** Xenotopic texture in calcite crystals from a calcite vein; **i** Epidote (ep) and calcite in a sheared ophicalcite

meta-cherts comprise alternations of dark and white lamellae. Dark-colored parts consist mostly of very fine-grained to cryptocrystalline phases, mainly hematite and pyrolusite, while the white ones are made of very fine-grained quartz, minor albite and chlorite. At places, quartz veinlets crosscut the lamination.

Ophicalcites

Serpentinitic clasts and the carbonate phase are the major constituents of the ophicalcites. Serpentinite clasts display characteristic mesh, hourglass and pseudomorphic textures (Fig. 5e, f). Antigorite crystals range in size between 0.01 and 2 mm and grow in random orientation. No olivine and/or pyroxene relics were found. The abundance of calcite and the existence of epidote, talc and chlorite (Fig. 5g–i) is a common characteristic. In some cases, especially nearby or within the shear zones, the serpentine crystals are elongated and subparallel, thus defining a lepidoblastic texture and foliation. In the carbonate-poor ophicalcites, serpentinitic clasts preserve bastite textures, which are rare in other ophicalcite types. Accessory phases include Cr-spinel, magnetite, chlorite and talc and are found in all ophicalcite types. Chromian spinel is often rimmed by magnetite; the latter occurs also disseminated as idiomorphic crystals (up to 0.5 cm). Rare sulfides (chalcopyrite, pyrite, sphalerite) are scarcely found in the carbonate veins, indicating that minor quantities of base metals were also transferred and deposited during the formation of the ophicalcites. Finally, small grains of epidote were found in the matrix of the serpentinitic mélange, along with hematite and magnetite.

The carbonate phase (Figs. 5g–i, 6a–c) is commonly represented by calcite, whereas rare dolomite is usually connected to tectonic fractures or shear zones. Calcite appears in coarse-grained white crystals forming typical xenotopic texture, and replaces antigorite, (Fig. 5h), with minor participation of talc, chlorite and tremolite (Fig. 5g). Inside the veins, calcite exhibits a crack-seal geometry, expressed by symmetric pairs of calcites growing towards the center of the fracture. Moreover, calcite developed along shear zones together with dolomite, minor epidote and actinolite (Fig. 5i) may show undulose extinction, due to deformation. Dolomite forms a mosaic of hypidimorphic crystals (up to 0.1 mm) and is restricted to

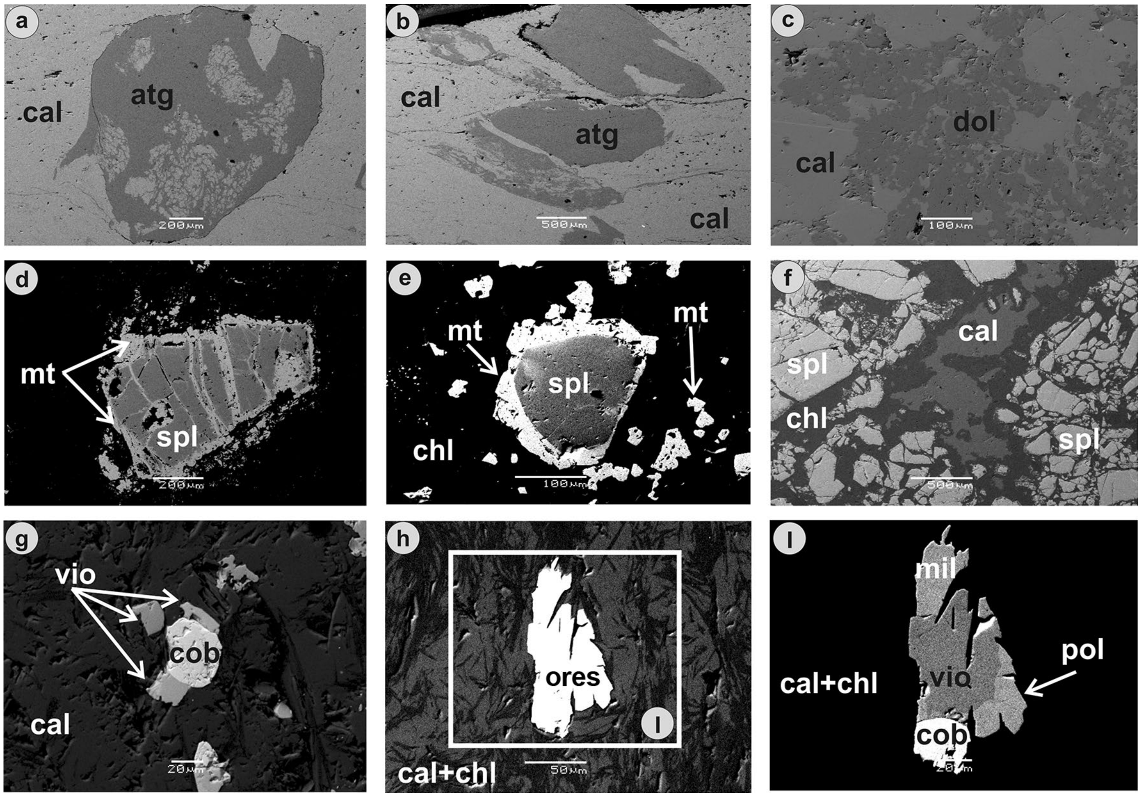

Fig. 6 SEM-BSE images of ophicalcites from Tinos island. **a**, **b** Calcite (cal) replacing antigorite (atg); **c** dolomite (dol) replacing calcite; **d** newly formed magnetite (mt) along the periphery and cracks of a Cr-spinel (spl) crystal; **e** Magnetite rimming spinel; **f** spinel cluster surrounded by calcite and Cr-chlorite (chl) in chromitite; **g**, **e**, **f** sulfides (millerite, polydymite and violarite) and sulfarsenide (cobaltite) from the chromitites: **g** coexisting violarite (vio) and cobaltite (cob) enclosed in calcite; **h**, **i** Intergrown millerite (mil), polydymite (pol), cobaltite (cob) and violarite (vio) in calcite–chlorite matrix of a chromitite

domains of intense tectonic stress, e.g., shear zones. These crystals replace pre-existing calcite.

Chromitites

The chromitites (up to 80 vol. % Cr-spinel) occur as pod-like, or irregular-shaped blocks reaching in size up to 2 m, and show intense cataclastic texture, with numerous fractures filled by coarse-grained calcite. Cr-spinel crystals are commonly replaced by magnetite, mainly at the periphery of individual grains or along fractures (Fig. 6d–f). Additional constituents comprise chlorite and minor antigorite and dolomite. In many cases, sulfarsenides (cobaltite) and sulfides (violarite, millerite and polydymite) occur in close spatial association with Cr-spinel (Fig. 6g–i). They are usually found as isolated grains or form intergrowths along with minor pyrite and chalcopyrite.

Mineral chemistry

Mineral-chemical data from the present study are summarized in Tables 1, 2, 3 and plotted for selected minerals in Fig. 7.

The chemical composition of antigorite displays minor variations: SiO_2 ranges from 42.26 to 44.74 wt %, FeO from 2.10 to 2.56 wt % and MgO from 37.94 to 39.07 wt %. In some samples, minor content of Al_2O_3 (up to 2.0 wt %) and NiO (up to 0.71 wt %) was measured (Table 1).

The carbonate phase is mostly represented by pure calcite; its MgO content occasionally reaches up to 4.22 wt %. (Fig. 7b). In some cases, minor FeO (up to 0.80 wt %) was detected. Calcite in the serpentinitic mélange tends to be richer in Fe compared to the other four ophicalcite types. Dolomite (MgO content between 18.0 and 20.8 wt %) was also identified (Table 1).

Chemical composition of Cr-spinels displays small variations: minimum Cr_2O_3 content is slightly higher in crystals from the chromitites compared to those disseminated in the ophicalcites, reaching values between 49.8 and 53 wt % and 48.08—53.8 wt %, respectively. FeO contents display small variations, with such grains in the chromitites being slightly poorer than those from the ophicalcites (values ranging from 15.05 to 24.13 wt % and 20.67 to 25.75 wt %, respectively, Tables 1 and 2). Al_2O_3 content in the Cr-spinels from ophicalcites ranges generally between 14.54 and 18.82 wt %. In

Table 1 Representative EPMA data from ophicalcite minerals: 1–3 antigorite; 4–5 calcite; 6 dolomite; 7–8 talc; 9–12 chlorite; 13–15 Cr-spinel; 16 magnetite

Wt.%		1	2	3	4	5	6	7	8	9	10	11	12	13	14	15	16
SiO_2		42.40	44.74	42.26	–	–	–	62.98	63.11	36.04	34.95	39.51	38.07	–	–	–	–
Al_2O_3		–	–	–	–	–	–	0.09	-	7.93	9.27	3.01	5.57	18.82	17.46	14.54	–
FeO		2.56	2.33	2.10	0.56	0.80	0. 60	1.24	1.13	2.35	1.78	7.02	1.09	20.67	25.75	22.69	88.34
MnO		–	–	–	0.11	–	–	–	–	–	–	–	–	–	–	–	–
MgO		37.94	39.07	38.12	0.38	4.22	20.80	30.08	31.16	34.42	33.75	32.44	39.05	11.04	8.99	8.94	–
CaO		–	–	–	51.87	47.82	30.61	–	–	–	–	0.12	–	–	–	–	–
Cr_2O_3		–	–	–	–	–	–	–	–	6.43	5.37	–	5.25	49.65	47.98	53.78	2.72
Total		82.90	86.14	82.48	52.71	52.84	52.01	94.39	95.40	87.17	85.12	81.97	88.33	100.54	100.18	99.95	91.06
Chemical formulae based on																	
		9 (O)			2 cations			22 (O)		28 (O)				4 (O)			
Si		2.659	2.690	2.658	0.000	0.000	0.000	8.064	7.996	7.355	7.481	7.032	6.944	0.000	0.000	0.000	0.000
Al	iv	0.000	0.000	0.000	0.000	0.000	0.000	0.001	0.000	0.519	1.085	0.968	1.056	0.685	0.661	0.553	0.000
	vi									1.820	0.717	0.859	0.750				
Fe^{2+}		0.134	0.117	0.110	0.002	0.003	0.002	0.131	0.122	0.401	0.319	1.187	0.176	0.467	0.570	0.565	1.915
Fe^{3+}		0.000	0.000	0.000	0.000	0.000	0.000	0.000	0.000	0.000	0.000	0.000	0.000	0.074	0.122	0.054	0.997
Mn		0.000	0.000	0.000	0.001	0.000	0.000	0.000	0.000	0.000	0.000	0.000	0.000	0.000	0.000	0.000	0.000
Mg		3.547	3.502	3.574	0.010	0.198	0.966	5.740	5.886	10.472	11.153	10.012	9.886	0.533	0.431	0.435	0.000
Ca		0.000	0.000	0.000	2.074	1.878	1.020	0.000	0.000	0.000	0.000	0.006	0.000	0.000	0.000	0.000	0.000
Cr		0.000	0.000	0.000	0.000	0.000	0.000	0.000	0.000	1.037	0.706	0.000	0.841	1.230	1.218	1.387	0.085

Table 2 Representative EPMA data from minerals of the chromitites: 1–5 spinel; 6–10 chlorite

Wt.%		1	2	3	4	5	6	7	8	9	10
SiO_2		–	–	–	–	–	35.44	33.70	35.22	34.00	35.63
Al_2O_3		16.96	17.27	17.67	16.90	17.01	6.07	6.84	5.53	6.33	7.30
Cr_2O_3		53.53	53.81	52.47	52.66	49.84	7.21	11.79	6.53	7.47	6.20
FeO		16.27	15.05	15.24	15.25	24.13	2.46	3.37	2.46	2.48	2.35
MnO		–	–	–	0.21	0.93	–	–	–	–	0.13
MgO		13.60	13.63	14.67	14.25	8.00	35.62	34.34	36.96	33.78	34.59
CaO		–	–	–	–	–	–	–	0.06	–	–
NiO		–	–	–	–	–	–	0.28	–	0.32	–
Total		100.36	99.76	100.03	99.27	99.91	86.80	90.04	86.78	84.29	85.97
Chemical formulae based on											
		4(O)					28 (O)				
Si		0.000	0.000	0.000	0.000	0.006	6.829	6.398	6.792	6.767	6.882
Al	iv	0.623	0.637	0.645	0.624	0.651	1.171	1.530	1.208	1.233	1.118
	vi						0.207	0.000	0.049	0.251	0.544
Cr		1.320	1.332	1.284	1.305	1.280	1.098	1.770	0.996	1.175	0.947
Fe^{2+}		0.368	0.364	0.323	0.329	0.587	0.396	0.535	0.400	0.391	0.342
Fe^{3+}		0.057	0.030	0.071	0.075	0.069	0.000	0.000	0.000	0.000	0.000
Mn		0.000	0.000	0.000	0.006	0.026	0.000	0.000	0.000	0.000	0.021
Mg		0.632	0.636	0.677	0.667	0.387	10.231	9.719	10.625	10.022	9.960
Ca		0.000	0.000	0.000	0.000	0.000	0.000	0.011	0.000	0.012	0.000
Ni		0.000	0.000	0.000	0.000	0.000	0.000	0.000	0.000	0.051	0.000

Table 3 Representative EPMA data of sulfarsenide (cobaltite) and sulfides (violarite, polydymite, millerite) from the chromitites: 1–2 cobaltite; 3–4 violarite; 5–6 polydymite; 7–8 millerite

Wt.%	1	2	3	4	5	6	7	8
As	47.21	47.43	–	–	–	0.10	–	–
Fe	0.89	0.91	14.03	13.87	15.17	13.15	1.01	0.95
Co	29.52	29.05	8.09	7.98	7.03	9.88	0.46	0.21
Ni	4.61	4.58	35.62	35.05	35.38	33.99	62.07	63.8
S	18.60	18.14	42.85	42.50	42.25	42.60	35.95	34.15
Total	100.83	100.11	100.59	99.40	99.83	99.62	99.49	99.11
	3 atoms		7 atoms		9 atoms		2 atoms	
As	1.047	1.034	0.000	0.000	0.000	0.002	0.000	0.000
Fe	0.027	0.027	0.754	0.755	1.074	1.019	0.016	0.015
Co	0.832	0.828	0.412	0.411	0.516	0.726	0.007	0.003
Ni	0.140	0.131	1.821	1.813	2.618	2.506	0.959	0.989
S	0.946	0.950	4.012	4.021	4.998	4.794	1.017	1.000

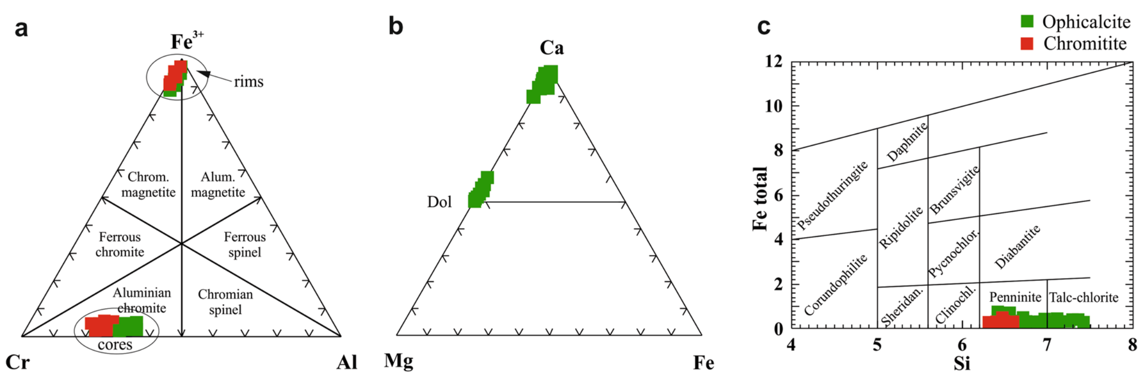

Fig. 7 **a** Trivalent cations plot of spinels after Stevens (1944); **b** carbonate compositions plotted in the ternary Ca–Mg–Fe diagram; **c** chlorite classification diagram after Hey (1954)

the case of the chromitites, the variance is slightly narrower (16.95–17.67 wt %). Trace impurities (ZnO, MnO and TiO_2) were detected in many cases (generally lower than 1 wt %). Chromite is commonly replaced in their outer rim by magnetite with moderate Cr_2O_3 concentration (up to 2.72 wt %) (Figs. 6d, e and 7a).

Chlorite commonly contains significant amounts of Cr (Tables 1 and 2) with the highest values measured in chlorites from the chromitites (up to 11.8 wt %). SiO_2 ranges significantly from 33.7 to 39.5 wt %. The FeO content is relatively homogeneous in all chlorites, ranging between 1.78 and 3.77 wt %. Al_2O_3 content is varying from 3.01 to 9.27 wt % in the chlorites from the ophicalcites; a smaller compositional range is observed in chlorites from the chromitites (5.53–7.3 wt %). Some chlorites contain traces of NiO, CaO, and Na_2O (up to 0.32 wt %, 0.16 wt %, and 0.10 wt %, respectively). According to the classification diagram (Fig. 7c), the analyzed chlorites from the ophicalcites plot in the fields of penninite and talc chlorite, while those from the chromitites display narrower compositional range and plot only in the field of penninite.

Talc forms veinlets in the studied ophicalcites, especially those of the upper part of the formation, but can also occur together with antigorite in carbonate-dominated veins representing "detrital" (disintegrated) material from the host rocks. Chemical analyses revealed almost stoichiometric compositions: SiO_2 ranges from 61.1 to 63.15 wt %, MgO from 30.38 up to 32.96 wt %. Minor presence of FeO that reaches up to 1.55 wt % was also measured in a few cases (Table 1).

Metallic minerals other than spinels comprise sulfides (millerite, violarite, polydymite) and the sulfarsenide cobaltite (Table 3 and Fig. 6g–i). Cobaltite shows significant substitution of Co by Ni; whereas, As and S are closer to stoichiometry. Violarite displays a small participation of Co (up to 0.412 apfu) that substitutes partly the Ni content and slight excess of S in the formula of the mineral, while polydymite and millerite display almost stoichiometric compositions.

Whole-rock chemical composition

Representative samples of serpentinites from the ophicalcites, metabasic rocks and a chlorite black-wall zone (chloritite) from the contact between ophicalcites and greenschists were analyzed by ICP-MS. Results are summarized in Table 4.

Serpentinites are typical ultrabasic rocks with SiO_2 ranging from 36.8 to 42.8 wt %, MgO from 30 to 35.9 wt %, and Fe_2O_3 from 7.01 to 8.43 wt %. Al_2O_3 is quite low, ranging from 0.44 to 2.08 wt%, while the CaO values, ranging from 0.07 to 8.06 wt %, possibly reflect the presence of certain amounts of fine-grained carbonates in the serpentinite clasts, especially when TOT/C is relatively high (e.g., samples TM45, TM49). TiO_2 values are extremely low (< 0.02 wt %) in all analyzed samples. Moreover, Cr_2O_3 (0.17–0.42 wt %), Ni (835–1973 ppm), Co (64–124 ppm), Zn (4–24 ppm), Cu (6–30 ppm) and As (2–9 ppm) show relatively high values and are related to the presence of base metal sulfides in the serpentinites. LOI values are relatively high in all samples ranging from 11.9 to 16 wt %.

Metagabbros are characterized by high SiO_2 and Al_2O_3 values that range from 51.95 to 59.85 wt % and 13.05–14.4 wt %, respectively. MgO content varies significantly from 6.14 to 11.61 wt %, while the Fe_2O_3 and CaO contents are relatively homogeneous, ranging from 5.26 to 7.43 wt % and 6.33–8.07 wt %. Metapyroxenites display quite distinct composition compared to the metagabbros, except for the SiO_2 values, which are in the same range (52.14–56.19 wt %). CaO and MgO contents are much higher, ranging from 12.48 to 18.74 wt % and 14.95–16.52 wt %, respectively, but Al_2O_3 and Na_2O are significantly lower, with values from 2.72 to 4.21 wt % and 0.34–1.59 wt %.

The chloritite is characterized by elevated Fe_2O_3, MgO and Al_2O_3 contents that reach 13.87 wt %, 24.82 wt %, and 17.95 wt %, respectively. SiO_2 is 29.68 wt % much lower compared to all other lithologies, while TiO_2 is 1.01 wt.%.

Trace and rare earth elements diagrams for all samples, normalized to primitive mantle and N-MORB after Sun and McDonough (1989), are shown in Fig. 8. Primitive mantle-normalized multi-element patterns of the analyzed serpentinites exhibit complex variations. Elements like Cs, U and Pb are strongly enriched, while Sr displays a moderate enrichment. Nb, Ce and Pr are highly depleted and HREE display a moderate depletion trend as well. Metagabbros and metapyroxenites follow, roughly parallel patterns, with metagabbros being slightly more enriched compared to the metapyroxenites. They are typically enriched in most of the elements, except for Nb which is strongly depleted and Ce, Pr and Sr which show minor depletion. Finally, the chloritite is characterized by strong Rb and Sr, and moderate Ba, Pb and P depletion, while Th, U, and the HREE display significant enrichment. In the NMORB-normalized diagram (Fig. 8b) the metabasites exhibit a large depletion in Nb relative to Th, with metagabbroic samples being slightly enriched in the majority of the trace elements, compared to the metapyroxenites. Both lithologies display relatively flat high field strength elements (HFSE) patterns. Most samples also record an enrichment in Rb, Ba, and a variable K content. The chloritite sample follows a distinct pattern compared to the metagabbros and metapyroxenites, characterized by depletion in large ion lithophile elements (LILE), especially in Rb, Ba, Sr, and K, while it is enriched in the HFSE.

Stable isotope (C, O) ratio

Oxygen and carbon isotope analyses were conducted on mineral separates of calcite (Table 5). Five samples are from vein-filling calcite, one sample is from a calcite clast, one sample comes from a reworked calcite clast and one sample was collected from a shear zone, which develops only in the internal part of the ophicalcites. $\delta^{18}O$ values range from 12.52 to 17.43 ‰ and form two groups. The $\delta^{13}C$ values display a relatively small variation, with two values clustering around 0 ‰ (− 0.25 ‰ and + 0.11 ‰), while most of the samples range between 2.16 and 2.55 ‰ (Fig. 9). It is notable that the two samples displaying the lowest $\delta^{13}C$ values, correspond to the highest $\delta^{18}O$ values. Comparing the Tinos data with other ophicalcite occurrences (Fig. 9), indicates that ophicalcites from elsewhere are characterized by lower $\delta^{13}C$ values, while most samples from Tinos fall slightly outside the range of other known ophicalcites (Table 5).

Discussion

Petrographic, geochemical and isotope characteristics

The studied ophicalcites are in many aspects similar to the Alpine ophicalcites as described by Bernoulli and Manatschal (2002). Based mainly on the extent of fracturing and carbonation, five ophicalcite types were distinguished. Four of these types (cataclastic, mega-clastic, mylonitic and carbonate-poor ophicalcites) are clearly of tectonic origin (OC1 type of Tricart and Lemoine 1989), as they consist of brecciated and/or sheared serpentinite which was subsequently cemented during consecutive episodes of hydrothermal alteration and calcite precipitation. One ophicalcite type is distinctly different, as it comprises a serpentinitic mélange (OC2 type, Tricart and Lemoine 1989). Although late shearing has obliterated most of the initial structures, apart from intense tectonism, relict sedimentary textures can be traced. Individual clasts with well-rounded shapes are embedded in a fine-grained matrix, suggesting reworking, transport and redeposition, for example, by a debris-flow mechanism. The

Table 4 Major (in wt. %) and trace element (in ppm) content of rock samples from the study area

Rock	Ophicalcite (Serpentinite clasts)					Metagabbro			Metapyroxenite		Chloritite
Sample	TM8	TM29	TM40	TM45	TM49	TM23	TM36	TM42	TM22	TM37	TM25
SiO_2	42.8	40.9	42.3	36.8	39.3	51.9	54.2	59.9	52.1	56.2	29.7
TiO_2	0.01	< 0.01	0.01	< 0.01	0.02	0.16	0.19	0.33	0.25	0.19	1.01
Al_2O_3	0.31	0.44	0.84	1.21	2.08	13.05	13.76	14.40	2.72	4.21	17.9
Fe_2O_3	7.48	7.35	7.38	7.01	8.43	7.43	5.74	5.26	7.01	7.46	13.9
MnO	0.08	0.09	0.07	0.10	0.07	0.14	0.12	0.10	0.17	0.12	0.24
MgO	35.9	35.2	35.9	30.0	32.5	11.6	9.95	6.14	16.5	14.9	24.8
CaO	0.39	1.95	0.07	8.06	3.08	8.07	8.35	6.33	18.74	12.48	0.73
Na_2O	< 0.01	< 0.01	< 0.01	< 0.01	0.01	3.18	3.49	6.14	0.34	1.59	< 0.01
K_2O	< 0.01	< 0.01	< 0.01	< 0.01	< 0.01	0.74	1.07	0.06	0.02	0.16	< 0.01
P_2O_5	< 0.01	< 0.01	< 0.01	< 0.01	< 0.01	0.01	0.02	0.02	0.01	0.01	0.01
Cr_2O_3	0.24	0.41	0.32	0.17	0.42	0.09	0.07	0.03	0.33	0.28	0.04
LOI	11.9	12.9	12.3	16.0	13.3	3.30	2.80	1.20	1.40	2.2	11.2
Total	99.18	99.18	99.17	99.38	99.14	99.73	99.77	99.86	99.65	99.84	99.55
Ni	1465	1366	1221	8345	1973	64	45	21	63	61	91
Sc	5	7	7	6	13	36	34	22	86	74	38
Ba	< 1	2	6	2	2	85	87	4	30	40	2
Be	< 1	< 1	3	2	< 1	< 1	< 1	< 1	2	na	< 1
Co	81	80	87	64	125	46	43	34	53	50	53
Cs	< 0.1	< 0.1	< 0.1	0.8	0.2	0.6	0.6	< 0.1	< 0.1	< 0.1	< 0.1
Ga	< 0.5	< 0.5	1	1	3	12	9	7	3	8	13
Hf	< 0.1	< 0.1	< 0.1	< 0.1	< 0.1	0.4	2	2	0.2	0.2	2
Nb	< 0.1	< 0.1	< 0.1	< 0.1	< 0.1	0.2	< 0.1	0.1	< 0.1	0.1	0.8
Rb	< 0.1	< 0.1	< 0.1	< 0.1	< 0.1	910	11	< 0.1	0.5	4	< 0.1
Sr	2	10	2	106	13	46	17	23	11	14	3
Ta	< 0.1	< 0.1	< 0.1	< 0.1	< 0.1	0.2	0.2	0.2	< 0.1	< 0.1	< 0.1
Th	< 0.2	< 0.2	< 0.2	< 0.2	< 0.2	0.2	< 0.2	0.3	< 0.2	< 0.2	0.5
U	< 0.1	0.2	< 0.1	< 0.1	0.7	< 0.1	< 0.1	0.1	< 0.1	na	0.2
V	19	15	17	34	57	133	105	86	244	196	224
W	36	20	39	8	30	137	175	143	143	140	2
Zr	2	0.3	0.5	2.4	0.6	14	53	48	4	14	62
Y	< 0.1	< 0.1	0.6	0.8	1	7	9	15	7	8	22
La	< 0.1	< 0.1	0.40	0.60	0.20	2	1	2	0.7	1	2
Ce	< 0.1	< 0.1	< 0.1	0.30	< 0.1	3	2	5	1	1	5
Pr	< 0.02	< 0.02	0.06	0.09	< 0.02	0.3	0.3	0.7	0.2	0.2	0.9
Nd	< 0.3	< 0.3	< 0.3	0.40	< 0.3	3	2	1	1	1	6
Sm	< 0.05	< 0.05	0.07	0.17	< 0.05	0.5	0.7	1	0.6	0.7	2
Eu	< 0.02	< 0.02	< 0.02	< 0.02	< 0.02	0.2	0.3	0.4	0.2	0.2	0.6
Gd	0.07	< 0.05	< 0.05	0.07	< 0.05	1	1	2	0.9	0.9	3
Tb	< 0.01	< 0.01	< 0.01	< 0.01	< 0.01	0.1	0.2	0.4	0.2	0.1	0.6
Dy	< 0.05	< 0.05	< 0.05	0.07	< 0.05	1	2	3	1	1	4
Ho	0.03	< 0.02	< 0.02	0.03	0.03	0.3	0.3	0.6	0.3	0.2	1
Er	< 0.03	< 0.03	0.08	0.03	0.1	0.7	1	2	0.8	0.8	3
Tm	0.01	< 0.01	0.01	< 0.01	0.03	0.1	0.2	0.2	0.1	0.2	0.4
Yb	0.10	< 0.05	0.07	0.23	0.2	0.8	1	2	0	0.7	2
Lu	< 0.01	< 0.01	0.02	< 0.01	0.04	0.1	0.1	0.2	0.1	0.1	0.3
Cu	15	8	13	6	30	17	8	39	178	78	33
Pb	< 0.1	0.3	2.3	0.6	0.6	4	1	0.5	4	2	< 0.1
Zn	6	4	5	24	17	26	12	8	8	9	42
As	3	9	2	2	4	< 0.5	< 0.5	< 0.5	1	na	0.7

Table 4 (continued)

Rock	Ophicalcite (Serpentinite clasts)					Metagabbro			Metapyroxenite		Chloritite
Sample	TM8	TM29	TM40	TM45	TM49	TM23	TM36	TM42	TM22	TM37	TM25
Au	< 0.5	1	< 0.5	0.6	0.8	< 0.5	< 0.5	1	3	na	< 0.5
TOT/C	0.2	0.5	0.1	2	0.7	0.1	0.1	< 0.02	0.1	na	< 0.02
TOT/S	< 0.02	< 0.02	< 0.02	< 0.02	0.12	< 0.02	< 0.02	< 0.02	< 0.02	na	< 0.02

na = not analysed

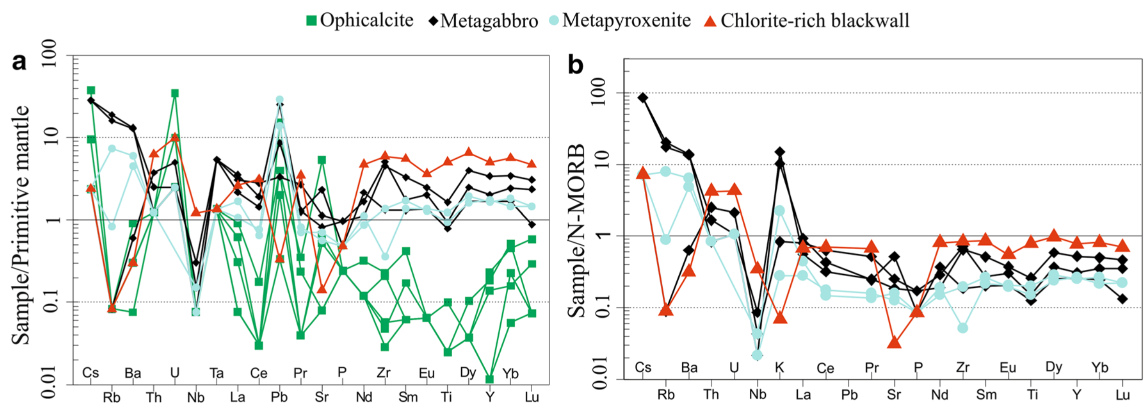

Fig. 8 Trace elements diagrams of the studied rocks, normalized to **a** primitive mantle and **b** N-MORB, after Sun and McDonough (1989)

Fig. 9 Isotope ratios of calcite from the Tinos ophicalcites compared to other Alpine occurrences (modified after Clerc et al. 2014)

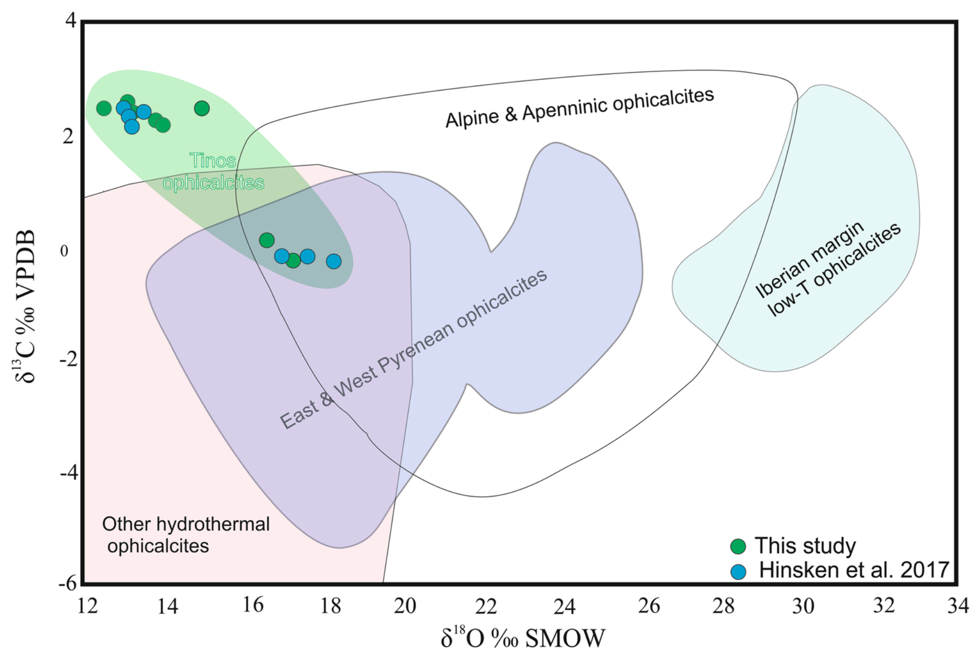

presence of hematite staining in parts of this ophicalcite type along with the presence of Fe-rich calcite, imply an oxidizing hydrothermal fluid. Calcite may have been precipitated from Fe- and/or Mn-enriched hydrothermal fluids discharging to the seafloor, that affected both the matrix-supported part of this rock and the sediments originally deposited nearby, leading to the formation of closely associated Mn-rich metasedimentary rocks. The oxidizing nature of the fluids is also supported by the assemblage of metallic minerals in the chromitites, which consists of millerite, polydymite cobaltite and violarite, while pyrrhotite and pentlandite are absent. Similar assemblage, characterized by the absence

Table 5 C–O isotopic values of calcite samples from the Tinos ophicalcites

Sample	Description	Ophicalcite type	$\delta^{18}O$ (‰ SMOW)	$\delta^{13}C$ (‰ VPDB)
TM1	Calcitic vein	Cataclastic	14.05	2.16
TM11	Calcitic vein	Mega-clastic	12.52	2.46
TM16	Calcitic vein	Mega-clastic	13.87	2.25
TM18	Calcitic vein	Cataclastic	17.43	−0.25
TM44	Calcitic clast	Cataclastic	16.77	0.11
TM48	Calcitic clast	Mega-clastic	13.29	2.39
TM52	Calcitic vein	Carbonate-poor	13.12	2.55
TM62	Calcitic vein	Mylonitic	15.03	2.46

of pyrrhotite and pentlandite, has also been described by Schwarzenbach et al. (2012), as indicative of oxidizing conditions.

The studied ophicalcites do not contain other rock components (e.g., gabbros, marbles etc.) than serpentinitic fragments and carbonate material. Textural observations, e.g., the bastitic pseudomorphs, and Al-poor bulk rock compositions suggest a dunitic and/or harzburgitic origin for the serpentinites, rather than lherzolitic. New and published geochemical data for the Tinos serpentinites indicate a relationship to a supra-subduction geotectonic regime (Fig. 10a, b), (e.g., Katzir et al. 1996; Stouraiti et al. 2017; Lamont et al. 2020; this study). These rocks are characterized by very low TiO_2 contents and thus clearly plot in the field of supra-subduction-oriented serpentinites (Pearce et al. 1984). Mineral-chemical data of Cr-spinels also suggest their formation in a supra-subduction environment (Fig. 10c, d), as expressed by their Al_2O_3 content compared to the Fe^{2+}/Fe^{3+} ratio. The presence of podiform chromitites in association with ophicalcites also points in this direction, because such mineralization is considered to form more likely in supra-subduction zone settings, than in a MOR spreading environment (Arai and Miura 2016 and references therein). Their formation also comprises multi-stage magmatic and deformation processes that involve Cr-rich melts and a dunite envelope (Boudier and Al-Rajhi 2014), which is indicated in the case of Tinos, by a fine-grained serpentinitic material that rims the chromitites.

Two-stage amphibole replacement of magmatic pyroxenes in metagabbros and metapyroxenites that occur closely associated with the ophicalcites in NW Tinos is similar to observations reported by Katzir et al. (1996) and Putlitz et al. (2001) for other occurrences of the UCU on Tinos: these rocks record deep sea, near-axis alteration of basic rocks by a sea water-derived hydrothermal fluid. The geochemical signature of the metabasic rocks from the Marlas area is analogous to other occurrences of metabasic rocks of the UCU (Stouraiti et al. 2017) and documents ocean-floor alteration (e.g., very high values of Pb, Rb and relative enrichment in K). The strong negative Nb anomaly in the Marlas metabasites, inferred as a subduction input proxy (Pearce 2014), was also reported by Lamont et al. (2020) for cumulate metagabbros of the Tsiknias area in the eastern part of Tinos. In addition to Nb, all trace element patterns of the Marlas cumulate gabbros, follow the same trend as that of the cumulate gabbros from Tsiknias Mt, suggesting that they should also be interpreted as fractional crystallization products and not primary mantle melts, forming from hydration and partial melting in a SSZ environment (Lamont et al. 2020).

$\delta^{18}O$ values of the carbonate components from the Tinos ophicalcites vary between 12.52 and 17.43 ‰, clustering into two groups, which are also characterized by different carbon isotope ratios (Fig. 9). Lower than marine carbonate $\delta^{18}O$ values have also been reported for the Pyrenean ophicalcites (Clerc et al. 2014). This $\delta^{18}O$ decrease implies introduction of externally derived fluids, which leads to extensive isotopic exchange between calcite and silicates (e.g., serpentine, talc), and is known as a metamorphic-driven alteration of the marine isotope signature of the ophicalcites (Weissert and Bernoulli 1984; Früh-Green et al. 1990; Clerc et al. 2014). In the case of Tinos, it clearly shows that extensive oxygen isotope resetting of the ophicalcites took place during their metamorphic history (see also Katzir et al. 1996), which can be attributed to exchange with adjacent minerals (serpentine, magnetite) and coexisting fluids at greenschist-facies temperatures.

Regarding the $\delta^{13}C$ values, most of the samples cluster between 2.16 and 2.55 ‰. This range is comparable with the $\delta^{13}C$ values of the Tinos marbles and suggest a marine carbon source, as also recorded by analogous data of Hinsken et al. (2017). The other two samples yielded $\delta^{13}C$ values around 0‰, comparable with $\delta^{13}C$ values measured in magnesite from the Tinos listvenites (Hinsken et al. 2017), suggesting a marine carbon source, which fits the scenario of interaction between ultramafics and seawater. However, this depletion in the $\delta^{13}C$ values implies that the precipitating fluids also included a magmatic CO_2 component.

Is there a genetic relationship between ophicalcites and listvenites?

The presence of either ophicalcites or listvenites in different parts of the UCU led Hinsken et al. (2017) to suggest that both rock types may form a continuous series of progressively carbonated ultramafic rocks. However, these authors finally rejected this hypothesis as supporting field observations or textural evidence for such a relationship were not recognized. Instead, Hinsken et al. (2017) considered it more plausible that the formation of ophicalcite and listvenite mostly took place in spatially and chemically different

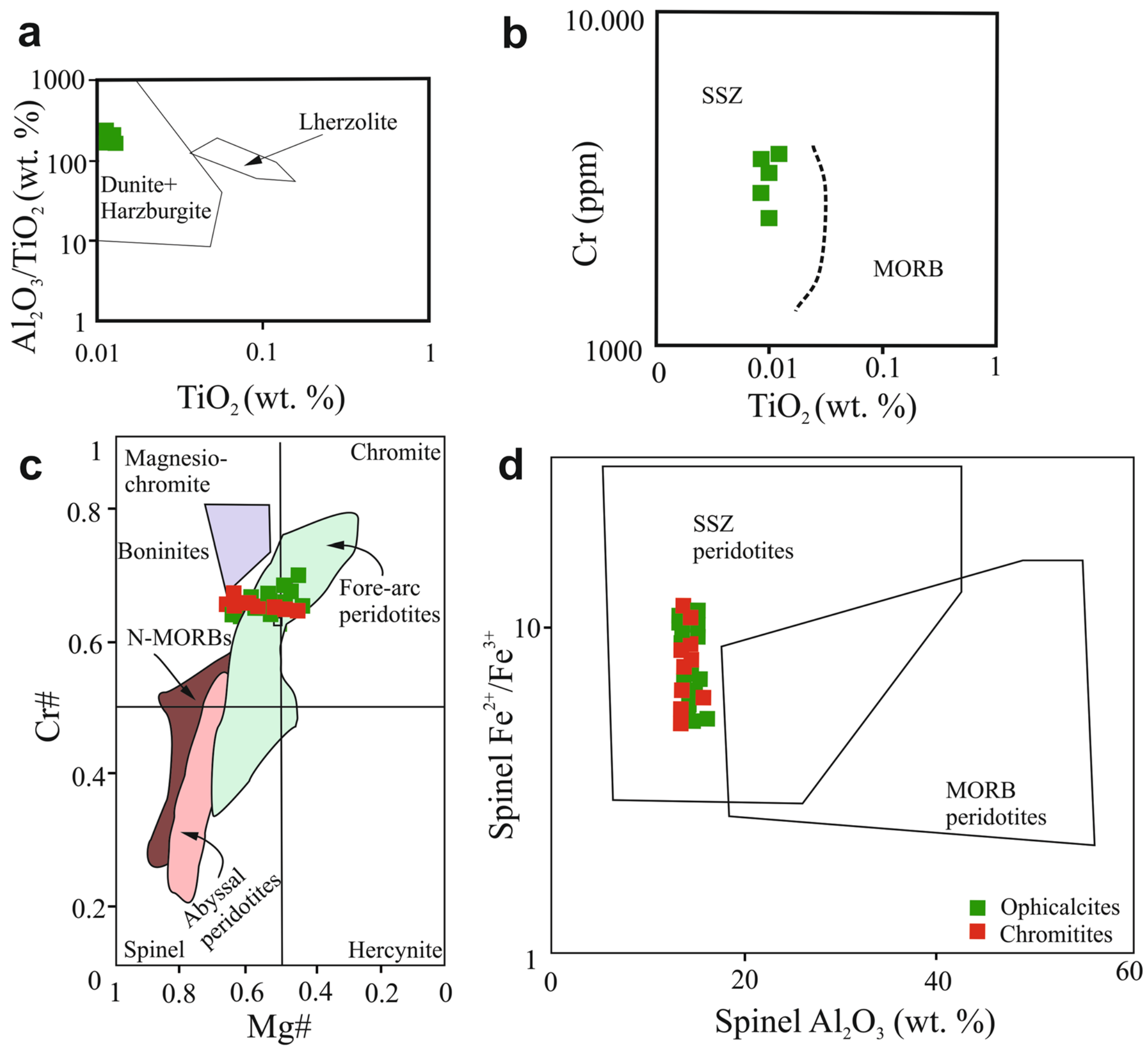

Fig. 10 **a** (Al_2O_3/TiO_2)–TiO_2 and **b** Cr–TiO_2 diagrams for the serpentinitic parts of Tinos ophicalcites after Beccaluva et al. (1983) and Pearce et al. (1984), respectively; **c** #Cr–#Mg geotectonic plot of Cr-spinels (fields after Dick and Bullen 1994; Ishii et al. 1992; Ohara and Ishii 1998); **d** Al_2O_3–(Fe^{2+}/Fe^{3+}) geotectonic plot

environments at distinctly different times. According to these authors, carbon and oxygen isotopes for the Tinos listvenite suggest that their formation results from deep circulation of marine fluids and their interaction with carbonate rocks (possibly the marbles present on Tinos) including a possible contribution from magmatic CO_2. Rb–Sr dating yielded an age of ca. 16–19 Ma for listvenitization, indicating that fluid infiltration took place after the tectonic juxtaposition of the UCU onto the CBU (Hinsken et al. 2017) which is considered to have taken place at ca. 21 Ma (Bröcker and Franz 1998). No ages are available for the calcite veins in the ophicalcites.

Based on their oxygen and carbon isotope ratios, Hinsken et al. (2017) distinguished two populations of calcite veins. One group was characterized by $\delta^{13}C$ values between 2.5 and 2.2‰ that are quite similar to the $\delta^{13}C$ values of Tinos marbles, suggesting a marine carbon source. The second group, however, yielded $\delta^{13}C$ values around 0‰ that are comparable to $\delta^{13}C$ values measured for magnesite of the listvenites. Furthermore, the oxygen isotope ratios of the ophicalcites is comparable/overlaps with those of listvenite from Tinos. Taken together, these data suggest broadly comparable conditions during fluid–rock interaction and a common fluid source, i.e., a seawater-dominated fluid at elevated temperatures (with a possible contribution of magmatic CO_2).

To develop a model for the formation of the Tinos ophicalcites, the following aspects must be considered: all listvenite outcrops occur close to a low-angle normal fault that separates the UCU from the CBU, suggesting a structural control on fluid infiltration and circulation (Hinsken et al. 2017). In contrast, the spatial distribution of the Tinos ophicalcites does not seem to correlate with the proximity to the tectonic contact. Other ophicalcite occurrences in Greece (e.g., Chasanbali area, mainland Greece; Melfos et al. 2009; Kati et al. 2009) also do not show a clear relationship to large-scale detachment fault systems. In NW Tinos, ophicalcite lenses occur in hinges of NE-trending, large-scale folds, parallel to those of the enclosing greenschists, thus suggesting that both rock types were together affected by orogenic deformation of the UCU during the Miocene (e.g., Katzir et al. 2007). As indicated by their ages, listvenites formed in their current setting by in situ carbonation of serpentinitic rocks. A strong argument for pre-emplacement ophicalcite formation is the complete absence of field observations indicating in situ carbonation. The ophicalcite bodies mainly exhibit cataclastic deformation of variable intensity that is not recorded in the other lithologies of the UCU. The fractures and fracture networks observed in the ophicalcites do not extend into the surrounding phyllites, which lack any indications for similar infiltration processes. These observations suggest that brittle deformation and carbonation of the ophicalcites occurred before their juxtaposition with the phyllitic rocks. Deformation in other lithologies of the UCU is mostly expressed through ductile to brittle features including schistosity, dilational jogs, double-sided mullions, and mineral segregations which can be related to the Miocene deformational event affecting both the UCU and the CBU. The ophicalcites largely escaped ductile deformation, except for shearing in the marginal parts of individual blocks. Further fracturing and/or reactivation of earlier fractures and shear zones could have occurred during this stage. Nevertheless, as evidence for in situ carbonation was not recognized, we consider it very likely that differences in deformation intensity and vein distribution between the various ophicalcite types are mostly inherited, documenting a continuous succession of upwards increasing fracturing and carbonation that happened in pre-Miocene time. Local modification by superimposed fracturing and non-pervasive fluid–rock interaction during Miocene and/or younger overprinting of the UCU cannot yet be ruled out.

An important question that remains to be answered is how and when the ophicalcite lenses (or their non-carbonated precursors) got emplaced into their current position within the UCU. Is this the result of tectonic mixing or the result of submarine gravity sliding? What is the protolith of the finely laminated metabasic phyllites: meta-tuffaceous rocks or highly deformed metabasalts? What is the protolith age of these rocks? Recently Lamont et al. (2020) suggested that the phyllites do not belong to the tectonically dismembered ophiolite suite (ca. 160 Ma), but are an integral part of an older metamorphic sole (ca. 190 Ma) and, thus, represent a rock suite with a partially different geological history.

Where and when did carbonation of the ophicalcites occur?

Trying to establish a possible genetic model for the Tinos ophicalcites carries a significant amount of uncertainty, because both metamorphism and deformation have caused significant obliteration of original features. However, detailed field and analytical work suggest that the Tinos ophicalcites may still record key information for unraveling their petrogenesis.

For further consideration, the definition of the original geotectonic setting where the hosting ophiolites formed is a prerequisite. Such information can be inferred from the whole rock and mineral geochemical characteristics of the studied rocks, which suggest a supra-subduction zone (back-arc) setting for the Tinos meta-ophiolites. Thus, any genetic models based on exhumation and carbonation of ultramafics at/near the seafloor in MOR-type settings, like the OCT environment (e.g., transition between Iberia and Newfoundland, Péron-Pinvidic and Manatschal 2009), or at fore-arc settings, where serpentine mud volcanoes form (e.g., Marianna trench, Fryer et al. 2020), are not applicable for the studied ophicalcites. The latter environment can also be excluded, since the fine-grained and mud-dominated texture of the serpentinitic volcanoes does not share common characteristics with the monomictic cataclastic breccia on Tinos.

The following explanations remain for the formation of the Tinos ophicalcites: (1) intra-oceanic transform fault zones, (2) obduction-related tectonic processes, and (3) low-angle normal (detachment) faults associated with oceanic core complexes (OCC).

Transform faults cutting across oceanic lithosphere can expose significant volumes of ultramafic rocks to the seafloor. Exhumation of the ultramafics in such domains is characterized by a succession of structural features that mark a transition from ductile to brittle deformation. A characteristic example is the São Paulo transform fault in the equatorial Atlantic Ocean (Barão et al. 2020). In such areas, ophicalcite breccias form in the final stages where brittle fracturing is superimposed on ductile (mylonitic) structures and is accompanied by carbonate precipitation, leading to the healing of the fractured serpentinites. Importantly, the absence of ductile features in the studied ophicalcites predating the fracture network is a critical piece of information that argues against the formation of the Tinos ophicalcites in an intra-oceanic transform fault zone. Moreover, in the case of Tinos the original oceanic architecture has been significantly disturbed, fact that makes it very difficult to identify the geometry of a transform fault zone, like for example the Arakapas transform fault in Troodos Massif (Simonian and Gass 1978). In this case, serpentinitic breccias also occur, however, they are not typical ophicalcites like those on Tinos.

An alternative scenario suggests that the ophicalcites formed because of obduction-related processes. The carbonated ultramafic rocks—listvenites from the Semail ophiolite (e.g., Falk and Kelemen 2015), are interpreted to be related to such processes, although no typical ophicalcites have been described from the area. This hypothesis can be reconciled with the interpretation of Katzir et al. (1996, 2007) and Putlitz et al. (2001) suggesting that regional metamorphism in the UCU was induced by early oceanic thrusting and piling of rock units with the suitable overburden to cause greenschist-facies metamorphism. This tectonic disturbance, an intra-oceanic thrusting inferred to have taken place soon after the formation of the oceanic suite (Katzir et al. 1996; Putlitz et al. 2001), could potentially produce ophicalcites by exposure of ultramafic rocks at the seafloor. However, such a thrusting generates an ophiolitic mélange (composed of ophiolitic and marine-sedimentary fragments in a wide range of sizes, embedded in a tectonized phyllitic or fine-clastic matrix) in the thrust front, as well as thinning of the overriding oceanic crust, both representing structures that are not documented in the UCU. Moreover, to our knowledge, formation of ophicalcites (in the form of the typical brecciated serpentinites, like those hosted on Tinos or other Alpine ophiolites) has not been reported elsewhere from such an environment. In addition, in case that ophicalcites were formed during the obduction of the oceanic crust, the other lithologies of the UCU (e.g., metagabbros, phyllites) should also exhibit carbonation, fact that is not documented on Tinos or any other UCU occurrence.

A more plausible scenario for the formation of the Tinos ophicalcites is the existence of a Mesozoic oceanic core complex in the Cycladic region. Intra-oceanic, low-angle normal (detachment) faults forming oceanic core complexes, commonly expose large-scale ultramafic rock units at the seafloor and in many cases leading to the formation of ophicalcites (Lemoine et al. 1987; Manatschal and Bernoulli 1999; Lavier and Manatschal 2006). Such complexes are known from the larger (Alpine) region and have been described, e.g., from the NW extension of the Greek ophiolites in Mirdita, Albania (Tremblay et al. 2009). Importantly, the actualistic example of the Godzilla Megamullion in the Philippine Sea, is related to a supra-subduction environment (Ohara 2016), similarly to Tinos. It should also be noticed that the overall deformation (e.g., the fracturing of the serpentinites that records extensional deformation that is missing from the other UCU lithologies, which mostly display compressional structures) recorded in the studied ophicalcites resembles the structural evolution of an area that once comprised the footwall of an oceanic detachment (Fig. 11).

Summary and conclusions

The ophicalcites of Tinos Greece, are associated with greenschist-facies metabasic phyllites of the Upper Cycladic Unit, together with other rock types representing a dismembered

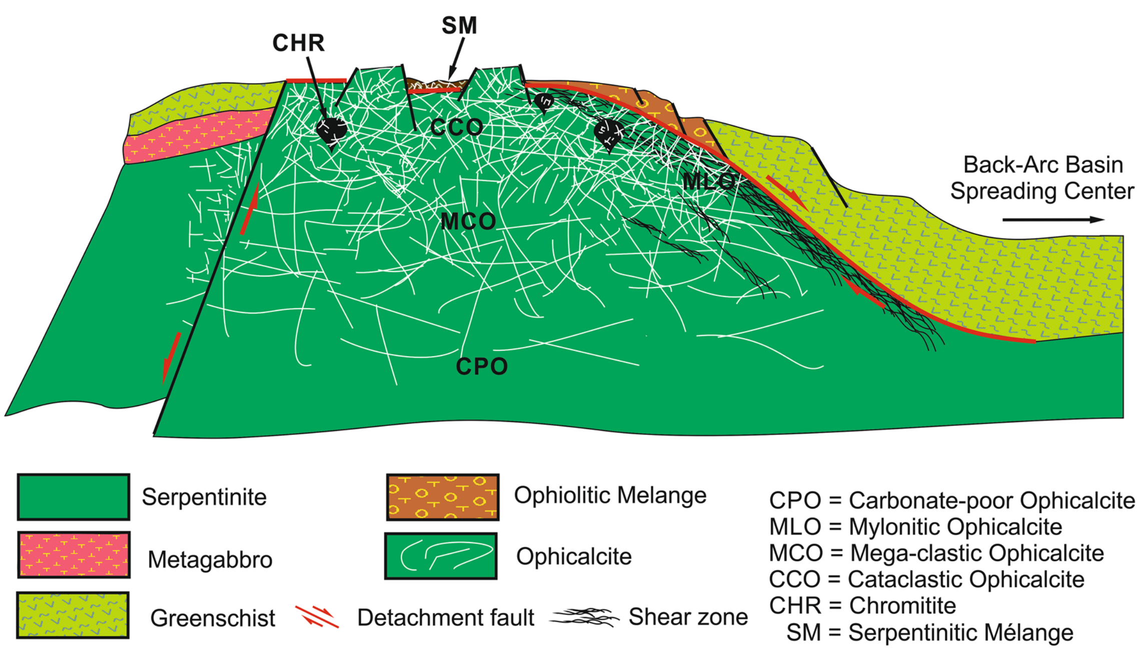

Fig. 11 Conceptualized sketch model for the formation of the Tinos ophicalcites

meta-ophiolitic complex. Ophicalcites occur as ENE elongated or ellipsoidal bodies, surrounded by zones of talc schists. Based on the extent of fracturing and carbonation, five ophicalcite types were distinguished. Four of these types (cataclastic, mega-clastic, mylonitic and carbonate-poor ophicalcites) are clearly of tectonic origin as they consist of brecciated and/or sheared serpentinite which has experienced consecutive episodes of hydrothermal alteration and calcite precipitation. One volumetrically subordinate ophicalcite type is distinctly different, as it comprises a serpentinitic mélange, indicating reworking, transport and redeposition. Differences in deformation intensity between the various ophicalcite types are mainly inherited, documenting a continuous succession of increasing fracturing and carbonation that mostly happened in pre-Miocene time. Mineralogically, the ophicalcites consist of serpentine minerals (mostly antigorite) and calcite; whereas, Cr-spinel, magnetite, dolomite, epidote, chlorite, talc, tremolite and actinolite are present as accessory phases. Fractured and carbonate-filled chromitites, which in some cases were found enclosed in the ophicalcites, consist of chromite partly altered to magnetite and Cr-chlorite. Talc schists, which usually separate the ophicalcites from the surrounding greenschists, mainly consist of talc with minor tremolite, actinolite and magnetite. Similar talc-rich assemblages were also identified in shear zones restricted to the interior of the ophicalcite lenses, implying the existence of inherited shear zones. Textural, mineralogical and geochemical data suggest that the serpentinitic part of the ophicalcites originated from harzburgite that formed in a supra-subduction zone setting. The isotopic signal records a significant disturbance due to metamorphism, expressed by decrease in their $\delta^{18}O$ values. Miocene in situ carbonation (as recognized for listvenites from the same tectonic unit) can be ruled out. Possible genetic models for the formation of the Tinos ophicalcites include an origin at intra-oceanic transform fault zones or low-angle normal (detachment) faults, the latter related to the existence of a fossilized oceanic core complex, or obduction-related processes. We consider it most likely that the origin of the ophicalcites is mainly related to cataclastic deformation and fracture-filling carbonation of serpentinized ultramafic rocks at/close to the seafloor, followed by reworking and redeposition of some parts of such bodies. The scenario that the ultramafic-gabbroic rock suite of the UCU on Tinos represents an oceanic core complex (OCC) seems the most possible. However, a further verification of this hypothesis, especially in the complex tectono-metamorphic framework of Tinos, is needed but this is beyond the scope of this article. In any case, the ocean-floor brecciation and hydrothermal alteration associated with the formation of the ophicalcites at or close to the seafloor should be considered as key factor in further investigation and refinement of this interpretation.

Acknowledgments Special thanks are due to Associate Professors S. Lozios and P. Pomonis for their valuable help on the field work and their useful advice on various matters, and Emeritus Professor A. Katerinopoulos for his kind help and support. The authors would also like to thank the Editor in Chief Prof. W.-C. Dullo, the topic Editor, an anonymous reviewer and Dr F. Zaccarini, for providing valuable comments that helped us to improve the manuscript.

References

Allen D, Seyfried WE Jr (2003) Compositional controls on vent fluids from ultramafic-hosted hydrothermal systems at mid-ocean ridges: an experimental study at 400°C, 500 bars. Geochim Cosmochim Acta 67:1531–1542

Altherr R, Kreuzer H, Wendt I, Lenz H, Wagner GA, Keller J, Harre W, Höhndorf A (1982) A late oligocene/early miocene high temperature belt in the attic-cycladic crystalline complex (SE Pelagonian, Greece). Geol Jb E23:97–164

Arai S, Miura M (2016) Formation and modification of chromitites in the mantle. Lithos 264:77–295

Artemyev DA, Zaykov VV (2010) The types and genesis of ophicalcites in Lower Devonian olistostromes at cobalt-bearing massive sulfide deposits in the West Magnitogorsk paleoisland arc (South Urals). Russ Geol Geophys 51(7):750–763. https://doi.org/10.1016/j.rgg.2010.06.03

Ashley KT, Caddick MJ, Steele-MacInnis MJ, Bodnar RJ, Dragovic B (2014) Geothermobarometric history of subduction recorded by quartz inclusions in garnet. Geoch Geophys Geosyst 15(2):350–360

Avigad D, Garfunkel Z (1989) Low angle faults underneath and above a blueschist belt—Tinos Island, Cyclades, Greece. Terra Nova 1(2):182–187

Avigad D, Garfunkel Z (1991) Uplift and exhumation of high-pressure metamorphic terrains: the example of the cycladic blueschist belt (Aegean Sea). Tectonophysics 188:357–372

Avigad D, Ziv A, Garfunkel Z (2001) Ductile and brittle shortening, extension-parallel folds and maintenance of crustal thickness in the central Aegean (Cyclades, Greece). Tectonics 20(2):277–287

Bach W, Früh-Green GL (2010) Alteration of the oceanic lithosphere and implications for seafloor processes. Elements 6(3):173–178. https://doi.org/10.2113/gselements.6.3.173

Bailey EB, McCallien WJ (1960) Some Aspects of the Steinmann Trinity, Mainly Chemical. Q J Geol Soc 116(1–4):365–395. https://doi.org/10.1144/gsjgs.116.1.0365

Baltatzis EG (1984) A new occurrence of ophicalcite from Paros Island. Neues Jahrb Miner Abh 150:325–329

Barão LM, Trzaskos B, Angulo RJ, de Souza MC (2020) Deformation and structural evolution of mantle peridotites during exhumation on transform faults: a forced transition from ductile to brittle regime. J Struct Geol 133:103981. https://doi.org/10.1016/j.jsg.2020.103981

Bargnesi EA, Stockli DF, Mancktelow N, Soukis K (2013) Miocene core complex development and coeval supradetachment basin evolution of Paros, Greece, insights from (U–Th)/He thermochronometry. Tectonophysics 595:165–182

Be'eri-Shlevin Y, Avigad D, Matthews A (2009) Granitoid intrusion and high temperature metamorphism in the Asteroussia Unit, Anafi Island (Greece): petrology and geochronology. Isr J Earth Sci 58:13–27. https://doi.org/10.1560/IJES.58.1.13

Beccaluva L, Di Girolamo P, Macciota G, Morra V (1983) Magma affinities and fractionation trends in ophiolites. Ofioliti 8:307–324

Bernoulli D, Jenkyns HC (2009) Ancient oceans and continental margins of the Alpine-Mediterranean Tethys: deciphering

clues from Mesozoic pelagic sediments and ophiolites. Sedimentology 56:149–190. https://doi.org/10.1111/j.1365-3091.2008.01017.x
Bernoulli D, Manatschal G (2002) Ophicalcites: tectono-sedimentary breccias related to mantle exhumation. In: Abstract volume of the Annual Meeting of the Swiss Academy of Natural Sciences, Davos, Switzerland, pp 15–16
Bernoulli D, Weissert H (1985) Sedimentary fabrics in alpine ophicalcites, South Penine Arosa zone. Geology 13:755–758
Bernoulli D, Manatschal G, Desmurs L, Müntener O (2003) Where did Gustav Steinmann see the Trinity? Back to the roots of an alpine ophiolite. In: Dilek E, Newcomb S (eds) Ophiolite concept and the evolution of geological thought
Boillot G, Froitzheim N (2001) Non-volcanic rifted margins, continental break-up and the onset of sea-floor spreading: Some outstanding questions. Geol Soc London Sp Publ 187(1):9–30. https://doi.org/10.1144/GSL.SP.2001.187.01.02
Bonney TG (1879) Notes on some Ligurian and Tuscan serpentinites. Geol Mag 6(2):362–371
Boudier F, Al-Rajhi A (2014) Structural control on chromitite deposits in ophiolites: the Oman case. Geol Soc Lond Spec Publ 392(1):263–277. https://doi.org/10.1144/SP392.14
Breeding CM, Ague JJ, Bröcker M, Bolton EW (2003) Blueschist preservation in a retrograded, high-pressure, low-temperature metamorphic terrane, Tinos, Greece: Implications for fluid flow paths in subduction zones. Geoch Geoph Geos 4:1–11. https://doi.org/10.1029/2002GC000380
Brichau S, Ring U, Carter A, Monié P, Bolhar R, Stockli D, Brunel M (2007) Extensional faulting on Tinos Island, Aegean Sea, Greece: how many detachments? Tectonics. https://doi.org/10.1029/2006TC001969
Bröcker M, Enders M (1999) U-Pb zircon geochronology of unusual eclogite-facies rocks from Syros and Tinos (Cyclades, Greece). Geol Mag 136:111–118
Bröcker M, Enders M (2001) Unusual bulk-rock compositions in eclogite-facies rocks from Syros and Tinos (Cyclades, Greece): implications for U–Pb zircon geochronology. Chem Geol 175:581–603
Bröcker M, Franz L (1998) Rb–Sr isotope studies on Tinos Island (Cyclades, Greece): additional time constraints for metamorphism, extent of infiltration-controlled overprinting and deformational activity. Geol Mag 135(3):369–382
Bröcker M, Franz L (2005) P-T conditions and timing of metamorphism at the base of the Cycladic blueschist Unit, Greece: the Panormos window on Tinos re-visited. Neues Jahrb Miner 181(1):91–93
Bröcker M, Keasling A (2006) Ionprobe U–Pb zircon ages from the high-pressure/low-temperature mélange of Syros, Greece: age diversity and the importance of pre-Eocene subduction. J Metam Geol. https://doi.org/10.1111/j.1525-1314.2006.00658.x
Bröcker M, Kreuzer H, Matthews A, Okrusch M (1993) $^{40}Ar/^{39}Ar$ and oxygen isotope studies of polymetamorphism from Tinos Island, Cycladic blueschist belt, Greece. J Metam Geol 11:223–240. https://doi.org/10.1111/j.1525-1314.1993.tb00144.x
Bulle F, Bröcker M, Gärtner C, Keasling A (2010) Geochemistry and geochronology of HP mélanges from Tinos and Andros, cycladic blueschist belt, Greece. Lithos 117:61–81
Cann J, Blackman D, Smith D et al (1997) Corrugated slip surfaces formed at ridge–transform intersections on the Mid-Atlantic Ridge. Nature 385:329–332. https://doi.org/10.1038/385329a0
Cannat M, Sauter D, Mendel V, Ruellan E, Okino K, Escartín J, Combier V, Baala M (2006) Modes of seafloor generation at a melt-poor ultraslow-spreading ridge. Geology 34(7):605–608
Clerc C, Boulvais P, Lagabrielle Y, de Saint BM (2014) Ophicalcites from the Northern Pyrenean belt: a field, petrographic and stable isotope study. Int J Earth Sci 103:141–163
Cornelius HP (1912) Petrographische Untersuchungen in den Bergen zwischen Septiner und Julienpass. Diss Neues Jahrb Miner 35:374–498
Cortesogno L, Galbiati B, Principi G (1981) Descrizione dettagliata di alcuni caratteristici affioramenti di brecce serpentiniche della Liguria orientale ed interpretazione chiave geodinamica. Ofioliti 6:47–76ed
Dick HJB, Bullen T (1994) Chromian spinel as a petrographic indicator in abyssal and alpine-type peridotites and spatially associated lavas. Miner Petrol 86:54–73
Dragovic B, Samanta LM, Baxter EF, Selverstone J (2012) Using garnet to constrain the duration and rate of water-releasing metamorphic reactions during subduction: an example from Sifnos, Greece. Chem Geol 314–317:9–22. https://doi.org/10.1016/j.chemgeo.2012.04.016
Dragovic B, Baxter EF, Caddick MJ (2015) Pulsed dehydration and garnet growth during subduction revealed by zoned garnet geochronology and thermodynamic modeling Sifnos, Greece. Earth Planet Sci Lett 413:111–122
Dürr S, Altherr R, Keller J, Okrush M, Seidel E (1978) The Median Aegean Crystalline Belt: Stratigraphy, structure, metamorphism, magmatism. In: Closs H, Roeder DH, Schmidt K (eds) Alps, apennines, hellenides. IUGS report no. 38, pp 455–77
Eickmann B, Bach W, Rosner M, Peckmann JL (2009) Geochemical constraints on the modes of carbonate precipitation in peridotites from the Logatchev Hydrothermal Vent Field and Gakkel Ridge. Chem Geol 268(1–2):97–106. https://doi.org/10.1016/j.chemgeo.2009.08.002
Engel M, Reischmann T (1998) Single zircon geochrology of orthogneisses from Paros Greece. Bull Geol Soc Greece 32(3):91–99
Escartín J, Smith DK, Cann J, Schouten H, Langmuir CH, Escrig S (2008) Central role of detachment faults in accretion of slow-spreading oceanic lithosphere. Nature 455:790–794. https://doi.org/10.1038/nature07333
Falk ES, Kelemen PB (2015) Geochemistry and petrology of listvenite in the Samail ophiolite, Sultanate of Oman: complete carbonation of peridotite during ophiolite emplacement. Geoch Cosmoch Acta 160:70–90
Florineth D, Froitzheim N (1994) Transition from continental to oceanic basement in the Tasna nappe (Engadine window, Graubünden, Switzerland): evidence for Early Cretaceous opening of the Valais Ocean. Schweiz Miner Petr Mitt 74:437–448
Folk RL, McBride EF (1976) Possible pedogeneic origin of Ligurian ophicalcite: a Mesozoic calichified serpentinite. Geology 4:327–332
Früh-Green GL, Weissert H, Bernoulli D (1990) A multiple fluid history recorded in Alpine ophiolites. J Geol Soc Lond 4:959–970
Fryer P (2012) Serpentinite mud volcanism: observations, processes and implications. Ann Rev Mar Sci 4:345–373. https://doi.org/10.1146/annurev-marine-120710-100922
Fryer P, Wheat CG, Williams T, Kelley C, Johnson K, Ryan J, Kurz W, Shervais J et al (2020) Mariana serpentinite mud volcanism exhumes subducted seamount materials: implications for the origin of life. Phil Trans R Soc A Math Phys Eng Sci. https://doi.org/10.1098/rsta.2018.0425
Fu B, Valley JW, Kita NT, Spicuzza MJ, Paton C, Tsujimori T, Bröcker M, Harlow GE (2010) Multiple origins of zircons in jadeitite. Contr Miner Petrol 159(6):769–780. https://doi.org/10.1007/s00410-009-0453-y
Gautier P, Brun JP (1994a) Ductile crust exhumation and extensional detachments in the central Aegean (Cyclades and Evvia Island). Geod Acta 7:57–85
Gautier P, Brun JP (1994b) Crustal-scale geometry and kinematics of late-orogenic extension in the central Aegean (Cyclades and Evvia Island). Tectonophysics 238:399–424

Groppo C, Forster M, Lister G, Compagnoni R (2009) Glaucophane schists and associated rocks from Sifnos (Cyclades Greece): new constraints on the P–T evolution from oxidized systems. Lithos 109:254–273. https://doi.org/10.1016/j.lithos.2008.10.005

Haggerty JA (1991) Evidence from fluid seeps atop serpentine seamounts in the Mariana forearc: clues for emplacement of the seamounts and their relationship to forearc tectonics. Mar Geol 102(1–4):293–309. https://doi.org/10.1016/0025-3227(91)90013-T

Hellenic Survey of Geology and Mineral Exploration, (2003) Map sheet 1:50.000 Tinos-Yaros

Hey MH (1954) A new review of the chlorites. Miner Mag 30:277–292

Hinsken T, Bröcker M, Strauss H, Bulle F (2017) Geochemical, isotopic and geochronological characterization of listvenite from the Upper Unit on Tinos, Cyclades, Greece. Lithos 282–283:281–297. https://doi.org/10.1016/j.lithos.2017.02.019

Ildefonse B, Blackman D, John B, Ohara Y, Miller DJ, MacLeod C (2007) Oceanic core complexes and crustal accretion at slow-spreading ridges. Geology 35:623–626

Ishii T, Robinson PT, Maekawa H, Fiske R (1992) Petrological Studies of Peridotites from Diapiric Serpentinite Seamounts in the Izu–Mariana Fore-Arc, Leg 125. In: Fryer P, Pearce JA, Stokking LB et al. Proceedings of the Ocean Drilling Program, Scientific Results, 125:445–485

Jolivet L, Patriat M (1999) Ductile extension and the formation of the Aegean Sea. In: Durand B, Jolivet L, Horvath F, Serrane M (eds): The Mediterranean Basins: tertiary extension within the Alpine Orogen. Geol Soc London Spec Publ 156:427–456

Jolivet L, Lecomte E, Huet B, Denèle Y, Lacombe O, Labrousse L, Le Pourhiet L, Mehl C (2010) The north cycladic detachment system. Earth Plan Sci Lett 289:87–104

Jolivet L, Faccenna C, Huet B et al (2013) Aegean tectonics: strain localisation, slab tearing and trench retreat. Tectonophysics 597–598:1–33. https://doi.org/10.1016/j.tecto.2012.06.011

Kati M, Magganas A, Melfos V, Voudouris P (2009) Sedimentology of the Larissa ophicalcite breccias: Mass flow deposits in a Tethyan Ocean-Continent Transition zone. Geophysical Research Abstracts, EGU General Assembly 2009 11, EGU2009-11002-1

Katsikatsos G, Migiros G, Triantaphyllis M, Mettos A, (1986) Geological structure of internal Hellenides. Geol Geoph Res Special Issue 191–212

Katzir Y, Matthews A, Garfunkel Z, Schliestedt M (1996) The tectono-metamorphic evolution of a dismembered ophiolite (Tinos, Cyclades, Greece). Geol Mag 133:237–254

Katzir Y, Garfunkel Z, Avigad D, Matthews A (2007) The geodynamic evolution of the Alpine orogen in the Cyclades (Aegean Sea, Greece): insights from diverse origins and modes of emplacement of ultramafic rocks. Geol Soc Lond Spec Publ 291:17–40. https://doi.org/10.1144/SP291.2

Kelley DS, Karson JA, Früh-Green GL, Yoerger D, Shank TM, Butterfield DA, Hayes JM, Schrenk MO, Olson E, Proskurowski G, Jakuba M, Bradley A, Larson B, Ludwig KA, Glickson D, Buckman K, Bradley AS, Brazelton WJ, Roe K, Elend M, Delacour AG, Bernasconi SM, Lilley MD, Baross JA, Summons RE, Sylva SP (2005) A serpentinite-hosted ecosystem: The Lost City hydrothermal field. Science 307:1428–1434

Klein F, Humphris SE, Guo W, Schubotz F, Schwarzenbach EM, Orsi WD (2015) Fluid mixing and the deep biosphere of a fossil Lost City-type hydrothermal system at the Iberia Margin. Proc Natl Acad Sci 112(39):12036–12041. https://doi.org/10.1073/pnas.1504674112

Lafay R, Baumgartner LP, Schwartz S, Picazo S, Montes-Hernandez G, Vennemann T (2017) Petrologic and stable isotopic studies of a fossil hydrothermal system in ultramafic environment (Chenaillet ophicalcites, Western Alps, France): processes of carbonate cementation. Lithos 294/295:319–338. https://doi.org/10.1016/j.lithos.2017.10.006

Lagabrielle Y, Cannat M (1990) Alpine Jurassic ophiolites resemble the modern central Atlantic basement. Geology 18(4):319–322. https://doi.org/10.1130/0091-7613(1990)018%3c0319:AJORTM%3e2.3.CO;2

Lagabrielle Y, Lemoine M (1997) Alpine, Corsican and Apennine ophiolites: the slow-spreading ridge model. Comptes Rendus de l'Académie des Sciences Series IIA Earth and Planetary Science 325(12):909–920. https://doi.org/10.1016/S1251-8050(97)82369-5

Lamont TN, Roberts NMW, Searle MP, Gopon P, Waters DJ, Millar I (2020) The age, origin, and emplacement of the Tsiknias Ophiolite Tinos Greece. Tectonics 39:e2019TC005677. https://doi.org/10.1029/2019TC005677

Lavier LL, Manatschal G (2006) A mechanism to thin the continental lithosphere at magma-poor margins. Nature 440:324–328

Lavoie D, Cousineau PA (1995) Ordovician ophicalcites of Southern Quebec Appalachians: a proposed early seafloor tectonosedimentary and hydrothermal origin. J Sed Res 65A:337–347

Lemoine M, Tricart P, Boillot G (1987) Ultramafic and gabbroic ocean floor of the Ligurian Tethys (Alps, Corsica, Appennines): in search for a genetic model. Geology 15:622–625

Ludwig KA, Kelley DS, Butterfield DA, Nelson BK, Früh-Green G (2006) Formation and evolution of carbonate chimneys at the Lost City Hydrothermal Field. Geoch Cosmoch Acta 70:3625–3645

MacLeod CJ, Searle RC, Murton BJ et al (2009) Life cycle of oceanic core complexes. Earth Planet Sci Lett 287:333–344

Maluski H, Bonneau M, Kienast JR (1987) Dating the metamorphic events in the Cycladic area: $^{39}Ar/^{40}Ar$ data from the metamorphic rocks of the island of Syros (Greece). Bull Soc Geol Fr 5:833–842

Manatschal G, Bernoulli D (1999) Architecture and tectonic evolution of nonvolcanic margins: Present-day Galicia and ancient Adria. Tectonics 18(6):1099–1119

Manatschal G, Müntener O (2009) A type sequence across an ancient magma-poor ocean-continent transition: the example of the western Alpine Tethys ophiolites. Tectonophysics 473:4–19. https://doi.org/10.1016/j.tecto.2008.07.021

Manatschal G, Müntener O, Desmurs L, Bernoulli D (2003) An ancient ocean-continent transition in the Alps: The Totalp, Err-Platta and Malenco units in the eastern Central Alps (Graubünden and northern Italy). Ecol Geol Helv 96:131–146

Martha SO, Dörr W, Gerdes A, Petschick R, Schastok J, Xypolias P, Zulauf G (2016) New structural and U-Pb zircon data from Anafi crystalline basement (Cyclades, Greece): constraints on the evolution of a Late Cretaceous magmatic arc in the Internal Hellenides. Int J Earth Sci 105(7):2031–2060. https://doi.org/10.1007/s00531-016-1346-8

Matthews A, Schliestedt M (1984) Evolution of the blueschist and greenschist facies rocks of Sifnos, Cyclades, Greece. A stable isotope study of subduction related metamorphism. Contrib Miner Petr 88:150–163

Matthews A, Lieberman JL, Avigad D, Garfunkel Z (1999) Fluid-rock interaction and thermal evolution during thrusting of an Alpine metamorphic complex (Tinos Island, Greece). Contr Miner Petrol 135(2):212–224. https://doi.org/10.1007/s004100050507

Mavrogonatos C, Magganas A, Kati M, Voudouris P (2014) Mineralogy and petrography of the NW Tinos Island ophicalcites, Cyclades, Greece. Bullet Shkencave Gjeol Special Issue 2

Mavrogonatos C, Magganas A, Kati M, Voudouris P (2015) Mineralogy and petrography of metagabbros and metapyroxenites from NW Tinos Island, Cyclades, Greece. Geoph Res Abstr 17, EGU2015-8922-1

Melfos V, Magganas A, Voudouris P, Kati M (2009) The Mesozoic Larissa Ophicalcite-Serpentinite Association in Eastern Thessaly, Greece: mineralogical, geochemical and isotopic constraints for rocks formed in an ocean-continent transition setting. Geoph Res Abstr 11, EGU2009-10797-2

Melidonis N (1980) Geological structure and are geology of Tinos Island (Cyclades), (in Greek). Special studies on the Geology of Greece, No 13, IGME

Ohara Y (2016) The Godzilla Megamullion, the largest oceanic core complex on the earth: a historical review. Island Arc 25:193–208. https://doi.org/10.1111/iar.12116

Ohara Y, Ishii T (1998) Peridotites from the southern Mariana forearc: heterogeneous fluid supply in the mantle wedge. Island Arc 7:541–558

Okrusch M, Bröcker M (1990) Eclogites associated with high-grade blueschists in the Cyclades archipelago, Greece: a review. Eur J Miner 2:451–478

Papageorgakis I (1966) Rocks suitable for marble sculpturing (in Greek). Ann Geol Pays Hell 18:193–270

Papanikolaou DJ (1979) Stratigraphy and structure of the Paleozoic rocks in Greece: an introduction. In: Sassi FP (ed) IGCP No. 5 Newsletter 1:93–102

Paraskevopoulos G, Kanaki F (1973) Genesis of the Greek ophicalcites (in Greek). Bull Geol Soc Greece 9:413–451

Patriat M, Jolivet L (1998) Post-orogenic extension and shallow-dipping shear zones, study of a brecciated decollement horizon in Tinos (Cyclades, Greece). Comptes Rendus de l'Académie des Sciences Series IIA Earth and Planetary Science 326:355–362

Patzak M, Okrusch M, Kreuzer H (1994) The Akrotiri unit on the island of Tinos, Cyclades, Greece: witness to a lost terrane of Late Cretaceous age. Neues Jahrb Geol Paläontol Abh 194:211–252

Pearce JA (2014) Immobile element fingerprinting of ofiolites. Elements 10(2):101–108

Pearce JA, Lippard SJ, Roberts S (1984) Characteristics and tectonic significance of supra-subduction zone ophiolites. In: Kokelaar BP, Howells MF (eds) Marginal Basin Geology. Geol Soc London Special Publ 16:77–94

Péron-Pinvidic G, Manatschal G (2009) The final rifting evolution at deep magma-poor passive margins from Iberia–Newfoundland: a new point of view. Int J Earth Sci 98:1581–1597

Peters T (1965) A water-bearing andradite from the Totalp serpentine (Davos, Switzerland). Am Miner 50:1482–1486

Philippon M, Brunn JP, Gueydan F (2011) Tectonics of the Syros blueschists (Cyclades, Greece): from subduction to Aegean extension. Tectonics 30:TC4001. https://doi.org/10.1029/2010TC002810

Picazo S, Cannat M, Delacour A, Escartín L, Rouméjov S, Silantyev S (2012) Deformation associated with the denudation of mantle-derived rocks at the Mid-Atlantic Ridge 13°–15° N: the role of magmatic injections and hydrothermal alteration. Geoch Geoph Geos. https://doi.org/10.1029/2012GC004121

Putlitz B, Katzir Y, Matthews A, Valley JW (2001) Oceanic and orogenic fluid–rock interaction in $^{18}O/^{16}O$-enriched metagabbros of an ophiolite (Tinos, Cyclades). Earth Planet Sci Lett 193(1):99–113. https://doi.org/10.1016/S0012-821X(01)00508-8

Ring U (2010) The Hellennic subduction system: High-pressure metamorphism exhumation, normal faulting, and large-scale extension. Ann Rev Earth Planet Sci 38:45–76. https://doi.org/10.1146/annurev.earth.050708.170910

Sánchez-Gómez M, Avigad D, Heimann A (2002) Geochronology of clasts in allochthonous Miocene sedimentary sequences on Mykonos and Paros Islands: implications for back-arc extension in the Aegean Sea. J Geol Soc Lond 159:45–60

Schwarzenbach EM, Früh-Green GL, Bernasconi SM, Alt JC, Shanks WC III, Gaggero L, Crispini L (2012) Sulfur geochemistry of peridotite-hosted hydrothermal systems: comparing the Ligurian ophiolites with oceanic serpentinites. Geochim Cosmochim Acta 91:283–305. https://doi.org/10.1016/j.gca.2012.05.021

Schwarzenbach EM, Früh-Green GL, Bernasconi SM, Alt JC, Plas A (2013) Serpentinization and carbon sequestration: a study of two ancient peridotite-hosted hydrothermal systems. Chem Geol 351:115–133

Seman S, Stockli DF, Soukis K (2017) The provenance and internal structure of the Cycladic Blueschist Unit revealed by detrital zircon geochronology, Western Cyclades Greece. Tectonics 36(7):1407–1429

Simonian KO, Gass IG (1978) Arakapas fault belt, Cyprus: a fossil transform fault. GSA Bull 89(8):1220–1230

Soukis K, Papanikolaou DJ (2004) Contrasting geometry between alpine and late-to postalpine tectonic structures in Anafi Island (Cyclades). Bull Geol Soc Greece 36(4):1688–1696

Soukis K, Stockli DF (2013) Structural and thermochronometric evidence for multi-stage exhumation of southern Syros, Cycladic islands, Greece. Tectonophysics 595–56:148–164. https://doi.org/10.1016/j.tecto.2012.05.017

Spooner ETC, Fyfe WS (1973) Sub-sea-floor metamorphism, heat and mass transfer. Contr Miner Petrol 42(4):287–304. https://doi.org/10.1007/BF00372607

Stevens RE (1944) Compositions of some chromites of the western hemisphere. Am Miner 29:1–34

Stouraiti C, Pantziris I, Vasilatos C, Kanellopoulos C, Mitropoulos P, Pomonis P, Moritz R, Chiaradia M (2017) Ophiolitic remnants from the Upper and Intermediate structural Unit of the Attic-Cycladic Crystalline Belt (Aegean, Greece): fingerprinting geochemical affinities of magmatic precursors. Geosciences 7:14. https://doi.org/10.3390/geosciences7010014

Sun S, McDonough WF (1989) Chemical and isotopic systematics of oceanic basalts: implications for mantle composition and processes. Geol Soc Lond Spec Publ 42:313–345. https://doi.org/10.1144/GSL.SP.1989.042.01.19

Surour AA, Arafa EH (1997) Ophicarbonates: calichified serpentinites from Gebel Mohagara, Wadi Ghadir area, Eastern Desert. Egypt J Afr Earth Sci 24(3):315–324

Tremblay A, Meshi A, Bédard JH (2009) Oceanic core complexes and ancient oceanic lithosphere: Insights from Iapetan and Tethyan ophiolites (Canada and Albania). Tectonophysics 473(1):36–52. https://doi.org/10.1016/j.tecto.2008.08.003

Tricart P, Lemoine M (1989) The *Queyras ophiolite* west of Monte Viso (Western Alps): indicator of a peculiar ocean floor in the Mesozoic Tethys. J Geodyn 13:163–181

Trommsdorff V, Evan BW, Pfeifer HR (1980) Ophicarbonate rocks: metamorphic reactions and possible origin. Archives des Sciences Genève 33:361–364

Weissert H, Bernoulli D (1984) Oxygen isotope composition of calcite in Alpine ophicarbonates: a hydrothermal or Alpine metamorphic signal? Eclogae Geol Helv 77(1):29–43

Whitmarsh RB, Beslier MO, Wallace PJ (eds) (1998) Proceedings of the Ocean Drilling Program, initial reports, vol 173. Ocean Drilling Program, College Station, p 493

Whittaker EJW, Zussman J (1956) The Characterization of Serpentine Minerals by X-ray Diffraction. Miner Mag 31:107–126

Zeffren S, Avigad D, Heimann A, Gvirtzman Z (2005) Age resetting of hanging wall rocks above a low-angle detachment fault: Tinos Island (Aegean Sea). Tectonophysics 400(1):1–25. https://doi.org/10.1016/j.tecto.2005.01.003